Cytosolic aspartate availability determines cell survival when glutamine is limiting

Hamza Furkan Alkan, MSc.

Massachusetts Institute of Technology

January 15th 2017 – January 15th 2018

SUPERVISORS

Matthew G. Vander Heiden, MD,PhD
Department of Biology
Koch Institute of Integrative Cancer Research
Massachusetts Institute of Technology

Juliane G. Bogner-Strauss, PhD
Department of Biochemistry
Graz University of Technology

TABLE OF CONTENTS

SUMMARY

Mitochondrial function is important for aspartate biosynthesis in cancer cells. Here, we show that mitochondrial aspartate export via aspartate-glutamate carrier 1 (AGC1) supports cancer cell proliferation and cellular redox homeostasis. Insufficient cytosolic aspartate delivery leads to amino acid and nucleotide depletion and cell death when TCA cycle carbon is reduced following glutamine withdrawal and/or glutaminase inhibition. Moreover, loss of AGC1 reduces allograft tumor growth that is further compromised by treatment with the glutaminase inhibitor CB-839. Together, these findings argue that mitochondrial aspartate export sustains cell survival in low-glutamine environments and AGC1 inhibition can synergize with glutaminase inhibition to limit tumor growth.

INTRODUCTION

Cancer cells are transformed from an organism's own cells and characterized by uncontrolled proliferation (growth) and invasion. Unlike normal cells, cancer cells constantly need to produce building blocks to make the new cell. Therefore, these cells have higher energetic and biosynthetic requirements. In order to meet these demands, proliferating cells take up more nutrient from environment and change their cellular metabolism to utilize these nutrients differently than non-proliferating cells. Cancer cells are often characterized by excess glucose uptake rate which is the basis of FDG-PET scanning for diagnosis. However, the usage of glucose is different in cancer cells compared to control cells. Although oxidative glucose catabolism is energetically the most efficient means to produce ATP, cancer cells often exhibit increased lactate production from glucose – also known as aerobic glycolysis (Lunt and Vander Heiden, 2011; Vander Heiden and DeBerardinis, 2017; Warburg, 1956). Instead, cancer cells often use glutamine as a primary carbon source to fuel tricarboxylic acid (TCA) cycle. Therefore, many proliferating cells in culture are vulnerable to glutamine withdrawal or glutaminase inhibition by drugs such as CB-839 (Gross et al., 2014; Yuneva et al., 2007).

After observing the prominent lactate production, German physiologist Otto Warburg hypothesized that mitochondrial dysfunction is the cause of cancer initiation(Warburg, 1956). However, although certain mitochondrial mutations were indeed shown to have tumorigenic effects, today it is better understood that mitochondrial function remains important for proliferating cells (DeBerardinis and Chandel, 2016). Mitochondrial one carbon metabolism is strongly up-regulated in several cancers to maintain purine and thymidine biosynthesis (Wei-Xing Zong, 2016; Vyas, 2016). Initiating de novo lipogenesis in mitochondria through citrate production is also vital for proliferation in some contexts. Another important role for mitochondrial respiration in proliferating cells is to support aspartate production, as aspartate is essential to make protein as well as for purine and pyrimidine biosynthesis (Birsoy et al., 2015; Gui et al., 2016; Sullivan et al., 2015). Because of the biosynthetic roles mitochondria acquire to support cell proliferation, movement of these macromolecule precursors across mitochondrial membrane could also become a limitation for tumorigenesis and proliferation. For instance, blocking mitochondrial citrate transporter impairs de novo lipogenesis and shown to inhibit cell proliferation is some contexts. In addition, maintaining the indirect transfer of electrons across cytosolic and mitochondrial compartments may also be important because accumulation of reducing equivalents in either compartments would lead to defects in proliferation. For instance, inhibiting mitochondrial electron transport leads to NADH accumulation in mitochondria, which inhibits oxidation reactions and impairs aspartate synthesis, causing growth arrest (Sullivan et al., 2015). Regenerating cytosolic NAD+ is also vital for glycolysis and the biosynthesis of certain amino acids and nucleotides (Lunt and Vander Heiden, 2011). Therefore it is important to expand our understanding on the role of mitochondrial transporters in proliferating cells for discovering novel targets to combat cancer. The Malate-Aspartate Shuttle (MAS) is a major mechanism for transferring electrons from cytosolic NADH to the mitochondria where they can be transferred to oxygen via the electron transport chain (Greenhouse and Lehninger, 1976, 1977). Exchange of mitochondrial aspartate for cytosolic glutamate and a proton by the Aspartate-Glutamate Carrier (AGC) is the only irreversible step of MAS (del Arco et al., 2002). Both AGC isoforms are predicted to be

functionally identical (Thangaratnarajah et al., 2014), yet many tissues selectively express one isoform: AGC1 (SLC25A12, Aralar) is abundant in brain, skeletal muscle, and pancreatic beta cells while AGC2 (SLC25A13, Citrin) is primarily found in liver and kidney (Begum et al., 2002; Palmieri et al., 2001). Previous studies have shown that AGC1 is involved in neuronal development, supports aspartate and N-acetylaspartate production and reduces lactate secretion (Jalil et al., 2005; Rubi et al., 2004).

Although MAS activity in tumors has been reported (Greenhouse and Lehninger, 1976, 1977) and the expression of AGCs in cancer has been predicted (Amoedo et al., 2016), the functional importance of aspartate-glutamate transport in proliferating cells has not been extensively studied. Here, we show that AGC1 knockdown slows cell proliferation, reduces NAD+/NADH ratio, and impairs aspartate delivery to the cytosol while lowering mitochondrial respiration and increasing pyruvate-to-lactate flux. We also show that mitochondrial aspartate export is essential for cell survival following glutamine starvation because it supports nucleotide biosynthesis. Loss of AGC1 can synergize with glutaminase inhibitors to slow cell proliferation and suppress syngeneic lung and pancreas allograft tumor growth. These findings argue that sustaining cytosolic aspartate levels is required for cell survival in low-glutamine conditions and suggest that AGC1 could be targeted as a novel approach to treat some cancers.

EXPERIMENTAL PROCEDURES

Cell Culture

All cells were sub-cultured in Dulbecco's Modified Eagle's Medium (DMEM, (25mM Glucose, 4mM Glutamine, 1mM Sodium Pyruvate) (GIBCO) supplemented with 10% fetal bovine serum and 50units/mL Penicilin/Streptomycin and incubated at 37°C with 5% CO_2. All cells utilized tested negative for Mycoplasma. AL1376 cell lines were derived from Kras^{G12D}; p53$^{fl/fl}$; Pdx-cre mouse models as described previously (Mayers et al., 2014).

Stable-knockdown of AGC1

Stable knock-down of AGC1 protein in C2C12 and LLC1 cells was achieved by using 5 independent mouse Slc25a12 mRNA targeting and 2 mammalian non-targetting lentiviral shRNA particles purchased from Sigma. For the transduction, 5 000 to 10 000 cells/well were seeded into 6-well plates. Following day, fresh media containing 8µg/mL Polybrene and a different lentivirus for each well (C2C12: 10MOI; LLC1: 6MOI). One well was incubated without lentivirus for selection control. After 3-4 days, cells were moved to T25 flasks; and selection was performed using varying concentrations of puromycin (C2C12: 0.75µg/mL; LLC1: 2,5µg/mL, AL1376: 4µg/mL) for 5-7 days until no viable cells remained in selection control.

Proliferation/Survival Rates

Cells were sub-cultured in standard DMEM until they reach to 50-60% confluence and then 25,000 cells/well (long term proliferation/survival experiments) or 100,000-200,000 cells/well (short term starvation, CB-839 treatment) were seeded into 6-well plates. After adhering overnight, initial cell number was determined from reference wells following trypsinization. Then the experimental wells were washed with PBS at least twice or once (only for LLC1 cells) and media conditions were applied. Due to low-adherent nature of LLC1 cells, both PBS and fresh media was applied very carefully. Final cell numbers were counted 2 or 3 days for C2C12 and LLC1 cells and 4 or 7 days AL1376, A549, H1299, PANC1, CAPAN2, HeLa cells after the treatment for proliferation experiments. Minimum 3mL media was used per well, 4 or 5mL media was used for incubations longer than 3 days. Proliferation/survival rate was calculated by the following formula

Proliferation/Survival Rate = Log_2 (Final cell count / Initial cell count) / Days

Cell Viability Assays

Cells were pre-grown the same manner as cell count assays. 500 (for growth assays) or 2,000 (for survival assays) cells were seeded into 96-well plates and allowed to adhere overnight. Media conditions (100µL/well) were applied as described above. After media change, 40µL (for survival) or 100µL (for proliferation) Cell Titer Glo (Promega) reagent was added into reference wells to get initial values for each replicate. Manufacturer's recommendations were followed to determine luminescence signals: plates were mixed for 2-3 minutes, incubated at

room temperature for 10 minutes and signals were measured using luminometer (Oreon II Microplate Reader Luminometer (Berthold)). Same protocol was used for final day measurements. For survival studies, final measurement was obtained after two or three days. For growth assays, media was refreshed every second day and final measurements were made at day four or five. The growth rate calculated by the following formula.

Proliferation/Survival Rate = Log_2 (Final measurement / Initial measurement) / Days

Transient overexpression of mouse and human AGC1

In order to investigate the effects of transient overexpression of murine AGC1 on proliferation, wild type C2C12 cells were grown till 50-60% confluence. Then, $0,5 \times 10^5$ cells were seeded into 1,5mL fresh media containing 6-well plates together with 1:1 mixture of 0.35µg pcDNA HisMax C vectors with or without AGC1 and 2µL Metafectane Pro (Biontex) -each diluted in 100µL serum free DMEM-. Media was refreshed after 24 hours and cells were counted 60-64 hours after transfection; and proliferation rate was calculated as described above.

To rescue AGC1-KD cells by expressing human AGC1, 70% confluent C2C12 cells were sub-cultured from T-75 flasks into 6-well plates while transfecting pHLCX vectors with or without human AGC1 (hAGC1). 12hours later, 2,000 cells were seeded into 96-well plates for cell viability assay. Media conditions were applied 8-12 hours later and final measurements were obtained 48hours after the reference measurements, as described above.

CRISPR/Cas9-mediated knock-out of AGC1

We cloned 7 different guide pairs targeting mouse AGC1 (sgAGC1) individually into lentiCRISPRv2 vector (Sanjana et al., 2014; Shalem et al., 2014) that includes Cas9-expressing cassette.

Then produced lentivirus using these vectors, as well as empty vector using HEK293T cells as described previously. In order to avoid selection pressures that could be caused by single-cell cloning process, we pooled the vectors containing vectors with different sgAGC1. Following lentiviral transduction, C2C12 cells were selected in the presence of 2mM pyruvate and 10mM aspartate.

Name of the guide	Target Sequence (5´-3´)
mSlc25a12_guide 1	GCCATGCTGTGCTCGGAAGC
mSlc25a12_guide 2	CCATGCTGTGCTCGGAAGCC
mSlc25a12_guide 3	CTCATGAGGATCACCTCGTT
mSlc25a12_guide 4	CAGGTGCATACAACCAAACG
mSlc25a12_guide 5	GGCTTCCGAGCACAGCATGG
mSlc25a12_guide 6	ACTCGCAGTCCCAGTTAAAA
mSlc25a12_guide 7	GGTTGTGCCCAAAGTGCAGC

siRNA-mediated knock-down of Got1/2

We obtained siRNA Universal Negative Control(SIC001) or MISSION esiRNA targeting mosue Got1 (EMU029631) or mouse Got2 (EMU094111) from Sigma-Aldrich. To deliver siRNAs into C2C12 cells, we used X-tremeGENE siRNA Transfection Reagent (Roche, 04476093001) following manufacturer's instructions. More specifically, we gently mixed 100pmol control siRNA or combination of Got1/Got2 esiRNA (50pmol each) with 200µL transfection reagent and applied them onto C2C12 cells that were previously grown to 50-60% confluency in 6-well plates. 8 hours later, cells were split into new 6-well plates as described for proliferation assays and media conditions were applied 2-hours after all cells were adhered.

NAD+/NADH Measurements

NAD+/NADH ratio measurement method was adopted from (Sullivan et al). 25,000 cells per well were seeded into 6-well plates using pyruvate-free DMEM, extracted in 120µL 1:1 0.2N NaOH:PBS solution after 24hours and frozen at -80°C immediately. For NADH measurement, 20µL lysate was incubated at 75°C for 30 min, during which oxidized NAD is degraded. For NAD+, 20µL lysate was diluted 1:1 with lysis buffer and 20µL 0.4N HCl was added. Later, NAD+ samples were incubated at 60°C for 15min to selectively degrade reduced form of NAD. After individual incubations, samples were cooled down to room temperature for 8 minutes and the degradation reactions were stopped by 20µL 0.25mM Tris in 0.2N HCl (NADH) and 0.5mM Tris base (NAD+). Manufacturer's instruction were followed after sample preparation (NAD/NADH Glo Assay, Promega).

Mitochondrial Oxygen Consumption

C2C12 cells were seeded in XF96 polystyrene cell culture microplates (Seahorse Bioscience®) at a density of 25.000 cells per well. 24 h after plating, cells were washed and preincubated for 30 min in serum-free XF assay medium supplemented with D-glucose (25 mM), sodium pyruvate (1 mM) and glutamine (2 mM) at 37°C in a non-CO2 environment. Oxygen consumption rate (OCR) was subsequently measured every 7 min using an XF96 extracellular flux analyzer (Seahorse Bioscience®). 2.5 µM antimycin A was used to stop mitochondrial respiration (=non-mitochondrial respiration). Basal mitochondrial oxygen consumption rate (OCR) was calculated by subtracting average of 3 subsequent non-mitochondrial OCRs from average of three basal OCRs (prior to antimycin treatment) and normalized to individual protein amount (pmol O2/(min x protein per well)).

For CB-839 treatment, 60,000 C2C12 cells were seeded in XF24-well plates and allowed to adhere overnight. Next day, wells were washed twice with PBS and serum-free, pyruvate-free DMEM, in the presence and absence of 1µM CB-839 (or 0.01% DMSO) were applied. 6 hours after treatment, OCRs were measured as described above and was subsequently normalized to cell counts and OCRs of individual genotype (control vs AGC1-KD) in DMSO treated conditions.

Metabolic Tracing and GCMS Analysis

For metabolic tracing studies 150,000-200,000 cells/well were seeded in 6-well plates to adhere overnight. Cells were washed three times and 5mM [U-^{13}C]glucose or 4mM [U-^{13}C]glutamine (Cambridge Isotopes Laboratories) containing DMEM (10% dialysed serum, no pyruvate) was applied. After 24h culturing, metabolites were extracted from cells or media (10µL) in 80% methanol in water containing 1µg/sample norvaline and dried under nitrogen gas. Polar metabolites were derivatized and measured using as described in (Lewis et al., 2014). Relative metabolite abundances were calculated by integrating ion peak area and normalized to norvaline and later to the cell numbers from identical plates. Mass isotopomer distributions of each ion peak were determined after natural abundance corrections adapted from (Fernandez et al., 1996).

Metabolic profiling using LCMS

For cells: 200,000 (in 6-well plate, for TCA intermediates and amino acids) (Corning) C2C12 cells were starved for glutamine in the absence or presence of 5mM Aspartate for 24hours. Samples were prepared using the same way as described in GCMS section. For tumors: each tumor was snap-frozen in liquid nitrogen immediately after harvesting and stored at -80°C. 6 tumors per group were selected randomly and ~10-20mg from each tumor were sampled and extracted in 80% methanol following the abovementioned procedure. Metabolites were quantified as detailed previously (Sullivan et al, Davidson et al) and described below.

Dried polar samples were resuspended in 50 µL water and 2 uL were injected into a ZIC-pHILIC 150 x 2.1 mm (5 µm particle size) column (EMD Millipore). Analysis was conducted on a QExactive benchtop orbitrap mass spectrometer equipped with an Ion Max source and a HESI II probe, which was coupled to a Dionex UltiMate 3000 UPLC system (Thermo Fisher Scientific, San Jose, CA). External mass calibration was performed using the standard calibration mixture every 7 days. Chromatographic separation was achieved using the following conditions: Buffer A was 20 mM ammonium carbonate, 0.1% ammonium hydroxide; buffer B was acetonitrile. The column oven and autosampler tray were held at 25°C and 4°C, respectively. The chromatographic gradient was run at a flow rate of 0.150 ml/min as follows: 0–20 min.: linear gradient from 80% to 20% B; 20–20.5 min.: linear gradient from 20% to 80% B; 20.5–28 min.: hold at 80% B. The mass spectrometer was operated in full-scan, polarity switching mode with the spray voltage set to 3.0 kV, the heated capillary held at 275°C, and the HESI probe held at 350°C. The sheath gas flow was set to 40 units, the auxiliary gas flow was set to 15 units, and the sweep gas flow was set to 1 unit. MS data acquisition was performed in a range of 70–1000 m/z, with the resolution set at 70,000, the AGC target at 10e6, and the maximum injection time at 20 msec. Relative quantitation of polar metabolites was performed with XCalibur QuanBrowser 2.2 (Thermo Fisher Scientific) using a 5 ppm mass tolerance and referencing an in-house library of chemical standards.

NMR Measurements

Sub-confluent C2C12 or LLC1 cells were incubated in 15cm dishes with pyruvate-free DMEM containing 5mM [U-^{13}C]glucose or 2mM [U-^{13}C]glutamine (Cambridge Isotopes Laboratories) for 12 hours. Next day, cells were washed twice and lysed in PBS via sonication. For quenching

the metabolites; one volume of cell lysate (or media) was mixed with two volumes of cold methanol, incubated at −20 °C for at least 1 hour, and centrifuged at 13000 rpm for 30 min to pellet proteins. Supernatants were transferred to fresh vials and dried for 4 hours at room temperature using speed vac. 500 µL of NMR buffer in D_2O were added to the samples, re-dissolved and transferred to 5 mm NMR tubes. Metabolites were measured as described previously(Prokesch et al., 2017; Radovic et al., 2016) and detailed below.

Methanol, sodium phosphate, dibasic (Na_2HPO_4), sodium hydroxide, hydrochloric acid (32 % m/v), and sodium azide (NaN_3) were obtained from VWR International (Darmstadt, Germany). 3(trimethylsilyl)propionic acid-2,2,3,3-d4 sodium salt (TSP) was obtained from Alfa Aesar (Karlsruhe, Germany). Deuterium oxide (D_2O) was obtained from Cambridge Isotope laboratories, Inc. (Tewksbury, MA). Deionized water was purified using an inhouse Milli-Q® Advantage Water Purification System from Millipore (Schwalbach, Germany). All chemicals were used with no further purification. The phosphate buffer solution was prepared by dissolving 5.56 g of anhydrous NaH_2PO_4, 0.4 g of TSP, and 0.2 g NaN_3, in 400 ml of deionized water and adjusted to pH 7.4 with 1M NaOH and HCl. Upon addition of deionized water to a final volume of 500 ml the pH was readjusted to pH 7.4 with 1M NaOH and HCl. The buffer was lyophilized and taken up in 500 ml D_2O to obtain NMR buffer in D_2O.

All NMR experiments were performed at 310 K on a Bruker Avance III 500 MHz spectrometer equipped with a TXI probe head. The 1D CPMG (Carr−Purcell−Meiboom−Gill) pulse sequence (cpmgpr1d, 512 scans, 73728 points in F1, 12019.230 Hz spectral width, 1024 transients, recycle delay 4 s), with water suppression using pre-saturation, was used for 1H 1D NMR experiments.

Bruker Topspin version 3.1 was used for NMR data acquisition. The spectra for all samples were automatically processed (exponential line broadening of 0.3 Hz), phased, and referenced to TSP at 0.0 ppm using Bruker Topspin 3.1 software (Bruker GmbH, Rheinstetten, Germany). The 2D HSQC (heteronuclear single quantum correlation) pulse sequence (hsqcetgpsisp2, 8 scans, 256 points in F1, 2048 points in F2, 12658.228 Hz spectral with in F1, 10026.738 Hz spectral width in F2) was used for 2D ^1H-^{13}C experiments. Spectral data were transferred to MestreNova 11.0.2 and processed (exponential line broadening of 0.3 Hz), phased, and referenced to TSP. Integral regions for metabolites of interest corresponding to a certain number of protons and for external standard were defined. Integrals were normalized to the number of protons and concentration was determined using external standard concentration. Concentrations of non-labelled compounds were determined using Chenomx NMR Suite 8.2 using internal standard concentration. For fold changes, the integral ratio of labelled vs. unlabelled compounds was calculated for each sample and replicates were averaged.

Immunohistochemistry

For AGC1 immunohistochemistry, Aralar B-2 antibody (Santa Cruz, sc-271056) (diluted 1:50 in Antibody Diluent Solution (Dako, S2022)) was applied on tissue slides that had been previously blocked with 3% H_2O_2 in methanol and incubated at room temperature for 1h. Afterwards, slides were covered with Rabbit/Mouse Detection Solution (Dako 5007) for 30min and subsequently stained with AEC Substrate Chromogen (Dako, K3464) and haematoxylin. Sections were imaged using light microscopy (Olympus) at given magnifications.

Allografts and *in vivo* CB-839 treatment

The study was approved by the institutional ethics committee and experiments were performed according to the guidelines of the Austrian Federal Ministry of Science and Research. Experiment licenses were granted under BMWF-66.007/0026-WF/V/3b/2015 and BMWF-66.007/0008-WF/V/3b/2016. In vivo CB-839 experiments were approved by the MIT Committee on Animal Care (IACUC). 500,000 LLC1 or 100,000 AL1376 cells were injected into flanks of 7-8 weeks old female C57BL/6 mice (Janvier and Jackson Laboratories). Tumor sizes were measured using calipers throughout the study and estimated volumes were calculated by using the formula $V = (\pi/6)*(length*width^2)$ (Gui et al., 2016). For CB-839 treatment studies, tumors were grown for 12 or 17 days followed by administration of 200mg/kg CB-839 or vehicle twice daily as previously described (Gross et al., 2014). Tumors were harvested 4 hours after the final drug dose and metabolites were quantified using LCMS.

Radioactive CO_2 Release

A day before measurements, 250,000 cells/well were plated into 6-well plates. 1.1µCi [U-^{14}C]-glutamine (ARC 0196) was added into each well and wells were covered with whatman paper soaked with 5M KOH. After incubating for 1h, wells were treated with 200µL of 2.6N $HClO_4$ for another 2h. Later, papers covering individual wells were cut gently and transferred into vials containing 20mL scintillation cocktail. Following rigorous shaking, radioactive carbon units were measured.

Extracellular Flux Analysis (YSI)

150,000-200,000 cells were seeded into 6-well plates and let adhere overnight. After 2 times washing, media conditions were applied (2ml/well) and cell counts were obtained from reference wells. 48 hours later, media samples were collected, centrifuged at top speed and stored at -80°C and final cell count were obtained from respective wells. Glucose, glutamine, lactate and glutamate concentrations were quantified using Metabolic Flux Analyzer (YSI 2900, YSI Life Sciences) in 96-well format.

Immunoblotting

Cells were harvested by scraping with SDS-lysis buffer (50 mM Tris-HCl, pH 6.8, 10 % glycerol, 2.5 % SDS, cOmplete^{TM} protease inhibitor cocktail) and samples were digested by benzonase (Merck Millipore). Protein concentrations were determined with the PierceTM BCA Protein Assay Kit (ThermoFisher Scientific). 15-50 µg of protein lysate were loaded into a 10% or 4-12% BisTris gel (NuPAGE, Invitrogen^{TM}, ThermoFisher Scientific), and gels were blotted to nitrocellulose membranes. Membranes were first blocked with 5%BSA in Tris-Buffered Phospohate Saline (TBST) and then incubated with Aralar B-2 (1:1000) (sc271056, Santa Cruz) and anti β-Actin (1:250000) (A5316, Sigma-Aldrich) antibodies (prepared in the same blocking solution) overnight at 4°C. Later, the primary antibodies were conjugated with horseradish peroxidase using secondary antibody (anti-mouse 1:5000) (Dako Österreich GmbH). SuperSignal™ West Pico Chemiluminescent Substrate (ThermoFisher Scientific, Waltham, MA, US) was used for detection.

Quantitative Real-Time PCR

PeqGOLD Total RNA Isolation Kit was used to extract RNA from cells (Peqlab). cDNA was synthesized using High Capacity cDNA Reverse Transcription Kit (Applied Biosystems). mRNA expression of individual genes was assessed using SYBR-green based qPCR method (Platinum SYBR Green qPCR SuperMix-UDG with ROX, Invitrogen) on a StepOne Plus Real-Time PCR System (Applied Biosystems) in 96-well format (96x0,2ml Plate, Frosted Subskirted Thin-wall) using 5pmol primer mixture and 5ng cDNA per well. Ct values of every gene first subtracted from the ones of TfIIβ and/or Rplp0 (δCt), then normalized to the mean δCt of control group for every gene (δδCt). Fold changes were calculated using the following formula: Fold change = $2^{-(\delta\delta Ct)}$

In experiments without control groups, such as comparing different cell lines, relative δCt values were projected in logarithmic scale, unless indicated otherwise.

Primers were obtained from Primer Bank Database (https://pga.mgh.harvard.edu/primerbank/). Pairs that yield smaller than 200bp amplicons and do not projected to amplify non-spesific regions were selected. Melting curve analysis was performed to verify specificity of the reactions. Primer sequences are available by request.

Determining Annexin V/Propidium Iodide staining using flow cytometry

150,000-200,000 cells were seeded into 6-well plates using full DMEM media. Next day cell were washed and media pyruvate-free DMEM with 4mM or 0.1mM glutamine was added. 24hours later cells were collected via trypsinization and stained with Annexin V and propidium iodide using Thermo Fischer Dead Cell Apoptosis Kit with Annexin V Alexa Fluor™ 488 & Propidium Iodide (PI) (V13241) to determine dead and apoptotic cells following manufacturer's instructions. Specifically, maximum 1 million/mL cells were diluted with annexin binding buffer after several washing steps and 5µL Alexa Fluor 488-Annexin PI and 1µL 100µg/mL PI solutions were added onto 100µL cell suspensions and incubated at room temperature for 15minutes. After the incubation period, 400µL of annexin-binding buffer was mixed gently with the cell suspension and immediately after fluorescence emmisons were measured in FITC (Annexin V) and Texas Red (PI) channels using flow cytometer (BD, FACS Diva). Cells positive with either of these dyes were determined and their abundance was analysed using FlowJo software.

Statistical analysis

Data are shown as mean ± standard deviation (SD) or mean ± standard error of the mean (SEM). Heat-maps denote medians. Sample size (n) indicates biological replicates within the same experiment. Statistics were calculated using two-tailed paired student's t-test unless indicated otherwise. Non-parametric t-test was used when the data within groups are not normally distributed or the sample size is larger than 6, otherwise parametric t-test was applied. Significance levels: * $p \leq 0.05$, ** $p \leq 0.01$, *** $p \leq 0.001$.

RESULTS

Knockdown of AGC1 reduces proliferation due to impaired aspartate synthesis

The aspartate-glutamate carrier 1 (AGC1) exports aspartate produced in mitochondria to the cytosol where it can be used for nucleotide, amino acid and protein synthesis. In addition to a biosynthetic role, exported aspartate can contribute to cytosolic redox homeostasis by serving as substrate for cytosolic glutamate-oxaloacetate transaminase (Got1, producing oxaloacetate from aspartate) and malate dehydrogenase (Mdh1, reducing oxaloacetate to malate while oxidizing NADH) as part of the malate-aspartate shuttle (MAS) (Figures 1A, S1A). mRNA expression analysis suggests that proliferating cells in culture display robust expression of MAS components (Figure S1B).

Considering the importance of the NAD+/NADH ratio and cytosolic aspartate availability for biosynthetic pathways, we hypothesized that aspartate export from the mitochondria could be important for cell proliferation. To test this hypothesis, we used shRNA to knockdown (KD) AGC1 in non-transformed mouse C2C12 myoblasts that have about 8-fold higher AGC1 mRNA expression than AGC2 (Figure S1B). We observed that AGC1-KD leads to a slight, yet significant, proliferation rate reduction in cells cultured in standard DMEM containing 1mM pyruvate (Figure 1B). Because extracellular pyruvate can act as an electron acceptor to provide oxidized NAD+ to cells (Figure 1A), we excluded pyruvate from the media for subsequent experiments unless otherwise indicated. The effect of AGC1-KD on cell proliferation becomes more apparent following pyruvate withdrawal and this change is rescued by pyruvate or aspartate supplementation (Figure 1C) as reported previously for cells with mitochondrial dysfunction (Birsoy et al., 2015; Sullivan et al., 2015). Interestingly, however, AGC1-KD cells remain viable and retain the ability to proliferate slowly in pyruvate-free media (Figure 1C).

AGC1 can be a rate-limiting component of the MAS, which is energetically the most efficient way to transfer reducing equivalents from the cytosol to mitochondria (del Arco et al., 2002). Disruption of the MAS is expected to decrease the NAD+/NADH ratio in the cytosol and increase the NAD+/NADH ratio in the mitochondria. Indeed whole cell NAD+/NADH ratio is lower in AGC1-KD cells compared to non-targeting control (NTC) cells hereafter referred to as control cells (Figure 1D). In addition, because the lactate dehydrogenase reaction is coupled to the cytosolic NAD+/NADH, the pyruvate/lactate ratio is sometimes used as a proxy for this ratio (Christensen et al., 2014; Williamson et al., 1967). As expected, AGC1-KD cells have a lower pyruvate/lactate ratio, consistent with the observed decrease in whole cell NAD+/NADH ratio (Figure 1E). Basal oxygen consumption rate is also lower in AGC1-KD cells (Figure 1F), a finding that is consistent with the expected increase in mitochondrial NAD+/NADH ratio. To determine whether AGC1-KD leads to similar phenotypes in transformed cells, we examined mouse Lewis lung carcinoma (LLC1) cells. As observed in C2C12 cells, AGC1-KD LLC1 cells proliferate slower than control LLC1 cells and have reduced NAD+/NADH and pyruvate/lactate ratio (Figure S1C-E).

The low NAD+/NADH ratio of AGC1-KD cells is accompanied by reduced aspartate levels in both LLC1 and C2C12 cells (Figure 1G, S1F). Because the enzyme asparagine synthetase (Asns) is predominantly localized in the cytosol (Ahn and Metallo, 2015), we examined how AGC1-KD affects asparagine levels, an amino acid produced from aspartate that is not present

in the culture media, to assess whether cytosolic aspartate is changed. Knockdown of AGC1 leads to reduced asparagine levels, further supporting that cytosolic aspartate is decreased in these cells (Figure 1G, S1F).

We also tested the effects of increased AGC1 expression, and found that overexpression of mouse AGC1 promotes C2C12 cell proliferation (Figure S1G). Increased expression of mouse AGC1 increases whole cell NAD+/NADH ratio and aspartate levels, opposite to what was observed following AGC1 knockdown using three independent shRNAs (Figure S1H-J). Furthermore, expression of human AGC1 (resistant to mouse shRNA) rescues the proliferation defect observed in AGC1-KD C2C12 cells (Figure S1K).

AGC1-KD increases cellular dependence on glutamine

We hypothesized that AGC1-deficient cells are able to maintain proliferation by rewiring metabolism to obtain cytosolic aspartate from a different source. To test this hypothesis, we individually removed glucose or select amino acids from the media and assessed whether this resulted in lethality upon AGC1 knockdown. We found that culturing cells in low glucose (0.5mM, instead of 25mM contained in regular DMEM) or with the glycolysis inhibitor 2-deoxglucose (2-DG) does not affect proliferation or survival of AGC1-KD cells more than control cells (Figure 2A). However, AGC1-KD cell survival was strongly reduced in Hanks' Buffered Salt Solution (HBSS) that contains 5.5mM glucose but lacks amino acids (Figure 2B). Addition of essential amino acids did not rescue this phenotype, but the addition of essential amino acids and glutamine to HBSS was able to rescue AGC1-KD cell proliferation to the same degree as control cells (Figure 2B). To further explore whether AGC1-KD alters dependence on glutamine, we cultured cells in low-glutamine (0.1mM instead of 4mM) DMEM-based media. In line with previous studies (Wise and Thompson, 2010), low glutamine strongly inhibits cell proliferation, but in contrast to control cells, AGC1-KD cell survival is compromised in low glutamine conditions (Figure 2C).

Glutamine has several fates in cells; it can serve as an exchange factor for import of other amino acids (Pochini et al., 2014), it provides nitrogen for nucleotide biosynthesis (Cory and Cory, 2006), or can be converted to α-ketoglutarate (α-KG or 2-oxoglutarate) via glutamate and provide carbon for TCA cycle intermediates (anaplerosis) (Wise and Thompson, 2010) (Figure 2D). To narrow down which fate of glutamine is important for proliferation and viability of AGC1-KD cells, we used the glutaminase inhibitor CB-839 to limit glutamine to glutamate conversion in mitochondria. We elucidated that AGC1-KD cells upon CB-839 treatment behave similarly to culture in a low-glutamine environment (Figure 2C), suggesting that nucleotide biosynthesis or other downstream reactions of glutamine that do not involve glutaminase are not limiting in the starvation experiments. Collectively, the data argue that AGC1-KD cells require glutamine anaplerosis for survival.

AGC1-KD suppresses reductive glutamine metabolism

We next hypothesized that increased vulnerability to glutaminase inhibition displayed by AGC1-KD cells could be due to the inability to oxidize glucose. To test this, we treated C2C12 cells for 6h with CB-839 and measured oxygen consumption. Interestingly CB-839 treatment reduces oxygen consumption rate by 50% in both AGC1-KD and control cells, arguing that

AGC1-KD cells do not require more glutamine for mitochondrial respiration than control cells. (Figure 3A). In addition, there is also no difference in the uptake or consumption rate of glucose and glutamine except that AGC1-KD C2C12 cells show slightly elevated glutamate release (Figure 3B, 3C, S2A-C). It is worth noting that only a small fraction of the consumed glutamine could be accounted for glutamate excretion in either group, suggesting that the glutamate excretion could be a consequence of an increased cytosolic glutamate pool in AGC1-KD cells and is not the cause of glutamine dependency. Consistent with this interpretation, exposure to Erastin, which inhibits plasma membrane glutamate exporter xCT (*Slc7a11*) (Dixon et al., 2014), has no specific impact on glutaminase-inhibited AGC1-KD cells (Figure S2D,E).

There are reports suggesting that changes in NAD+/NADH ratio can indirectly alter glutamine metabolism; in hypoxia or upon mitochondrial dysfunction, the canonical oxidative pathways are inhibited due to accumulation of reducing equivalents (Metallo et al., 2011; Sullivan et al., 2015; Mullen et al., 2014). In such conditions, increased conversion of glutamine-derived α-KG to citrate via isocitrate-dehydrogenase by reductive carboxylation is observed. Because AGC1-KD cells might display a different glutamine metabolism due to altered NAD+/NADH ratio, we traced $[U^{13}C]$glucose or $[U^{13}C]$glutamine fate using GC-MS. We did not observe a major change in nutrient utilization such that glutamine remains the predominant source of aspartate and other TCA intermediates and the relative contribution of glucose and glutamine to the TCA cycle is not drastically altered in AGC1-KD cells (Figure S2F-G). However, in alignment with a high mitochondrial NAD+/NADH ratio, AGC1-KD C2C12 cells display decreased M+5 citrate and M+3 aspartate from labeled glutamine, consistent with decreased reductive carboxylation (Figure 3D, 3E, 3I). Moreover, at steady state, M+3 species of α-KG and glutamate are increased while M+5 species are decreased in AGC1-KD C2C12 cells without any apparent differences observed in unlabelled (M+0) species (Figure 3F, 3G, 3I). These patterns point out a higher mitochondrial NAD+/NADH ratio promoting increased oxidative TCA cycling. Consistent with this interpretation, AGC1-KD C2C12 cells release higher amounts of ^{14}C-CO_2 from $[U^{14}C]$glutamine (Figure 3H, 3I). Interestingly, we did not observe the same decrease in reductive carboxylation in LLC1 cells with AGC1 knockdown (Figure S2G). This suggests that changes in reductive carboxylation are not the only reason why AGC-KD cells require glutamine *in vitro*. Together, these findings argue that glutamine utilization is not drastically altered in AGC1-KD cells, and that glutamine remains the major precursor for aspartate independently of AGC1 expression (Figure S2F-G).

AGC1-KD cells are unable to sustain cytosolic aspartate levels, leading to cell death upon glutamine-deprivation

Cytosolic aspartate production is essential for cell survival when mitochondria are dysfunctional (Birsoy et al., 2015), pointing out the importance of maintaining cytosolic aspartate levels. Because labeling studies in glutamine-replete media were insufficient to explain increased glutamine dependency of AGC1-KD cells, we hypothesized that the export of residual aspartate from mitochondria might be crucial for survival following glutamine starvation. In fact, AGC1 protein accumulates upon glutamine deprivation (Figure 4A). We speculate that glutamine withdrawal depletes mitochondrial aspartate levels to a local concentration where other mitochondrial transporters cannot bind and export it efficiently and cells may try to maintain cytosolic delivery by increasing the amount of AGC1 (Figure 4B). To

test whether cytosolic aspartate delivery that can be limiting for AGC1-KD cells in low glutamine, we provided cells with exogenous aspartate. Strikingly, aspartate supplementation in low-glutamine media completely rescues AGC1-KD cell viability, suggesting that cytosolic aspartate delivery can be limiting for AGC1-KD cell proliferation/survival (Figure 4C, S3A). Because aspartate is poorly permeable to the cells, we needed to use 5-20mM aspartate to achieve consistent rescues. However, expressing plasma membrane aspartate transporter made 150µM (RPMI levels) of aspartate be sufficient to rescue low-glutamine (Figure S4B), suggesting that it was not over-abundance of aspartate that promotes proliferation/survival.

The synergy between AGC1 loss and glutamine metabolism is consistent across other cell lines tested and can be rescued by aspartate, suggesting that these findings were also generalizable beyond C2C12 and LLC1 cells (Figure 4C). However, cell lines showed varying responses to glutamine starvation, glutaminase inhibition, AGC1 knockdown and/or aspartate rescue (Figure 4C), particularly pancreas cancer cell lines appear more resistant to CB-839 treatment than lung cancer cells. In addition, CRISPR/Cas9 mediated knock-out of AGC1 leads to a comparable sensitivity to perturbations that limits glutamine metabolism in C2C12 cells (Figure S4C). Interestingly, similar to partial knock-down, total ablation of AGC1 also did not completely block proliferation in glutamine-replete media, suggesting that some cytosolic aspartate delivery could still be maintained by AGC2 or other mitochondrial transporters when mitochondrial aspartate production is high. It is also important to note that, glutamate supplementation failed to completely rescue AGC1-KD cells in low glutamine, suggesting that a potential reduction in mitochondrial glutamate uptake may be one factor exacerbating the dependence on mitochondrial glutamine anaplerosis of AGC1-KD cells (Figure S4D-E).

We also measured cell death using Annexin V/promidium iodide (PI) staining. Glutamine starvation (0.1mM) significantly increased the percent of dead and apoptotic cells both in control and, to a higher extend, in AGC1-KD cells (Figure S3F). Interestingly, AGC1-KD also induced cell death in glutamine-replete media which is further exacerbated with glutamine starvation (Figure S3F). Furthermore, cleaved caspase 3 levels, a marker of apoptotic cells, were increased in low glutamine, suggesting that glutamine starvation induce programmed cell death (Figure S3G).

Collectively, these data suggest that AGC1-KD could synergize with glutaminase inhibitors in several cell lines and that cytosolic aspartate unavailability can significantly impair proliferation/survival when glutamine anaplerosis is inhibited.

AGC1-KD cells require high mitochondrial aspartate levels to maintain aspartate export

We then hypothesized that AGC1-deficient cells are addicted to high mitochondrial aspartate levels in order to maintain sufficient aspartate delivery to cytosol. Accordingly, AGC1-KD cells could be also vulnerable to any other perturbations that would deplete mitochondrial aspartate, similar to glutamine withdrawal. For instance, metformin blocks mitochondrial aspartate production by inhibiting mitochondrial complex I and disrupting NAD+/NADH ratio (Sullivan et al., 2015) (Figure 5A) and AGC1-KD cells are more sensitive to metformin treatment than control cells (Figure 5B), implying that synthetic lethality of AGC1-KD cells could be associated with the drops in mitochondrial aspartate levels.

In the same regard, supplementing other anaplerotic carbon sources would increase mitochondrial aspartate production through fueling TCA cycle. Pyruvate can fuel the TCA by

entering the cycle from 2 different positions; as four and two carbon substrates through pyruvate carboxylase and pyruvate dehydrogenase reactions, respectively. Pyruvate carboxylase (PC) deficiency is synthetic lethal with glutamine-withdrawal, because a source of anaplerotic carbon is required for survival (Cheng et al., 2011). Similarly, cell permeable dimethyl alpha-ketoglutarate (daKG) can rescue glutamine limitation as it can deliver the same five carbon units to mitochondria via by-passing glutaminase step. As expected, daKG and pyruvate supplementation significantly improves proliferation/survival of AGC1-KD cells in glutamine limitations (Figure 5C, S4A-B) by increasing aspartate levels (Figure 5D, S4C-D).

These findings suggest that inhibition of glutamine anaplerosis, the predominant aspartate source, decreases mitochondrial and cytosolic aspartate levels, leading to growth inhibition in wild-type cells. In AGC1-KD cells however, the inability to export residual aspartate from mitochondria further reduces cytosolic aspartate and further compromises cell proliferation/survival unless exogenous aspartate or other anaplerosis sources are provided (Figure 5E, 5G).

Cytosolic aspartate is essential for nucleotide biosynthesis but not for non-essential amino acids or TCA cycle

Next, we investigated what the cytosolic aspartate could be most limiting for when glutamine anaplerosis is inhibited. Aspartate is a non-essential proteinogenic amino acid that is also involved in several metabolic pathways beyond its use for protein translation, some of which have been reported to be associated with cell proliferation (Figure 6A, S5A). Cytosolic aspartate could undergo transamination to 1) support non-essential amino acid (NEAA) synthesis, 2) to deliver four carbon units to mitochondria for TCA cycle or 3) recycle NAD+ through cytosolic part of MAS. In addition to transamination related paths, it 4) accepts amide nitrogen from glutamine for asparagine biosynthesis, 5) is essential for both purine and pyrimidine biosynthesis and 6) is acetylated to produce N-acetylaspartate (NAA), a brain metabolites that is also found to have roles outside central nervous system (Figure 6A). Although NAA was recently reported to have beneficial effects on cell survival in some cancer cells, we failed to detect endogenous NAA in either C2C12 or LLC1 cells, suggesting cytosolic aspartate may not be a limitation for this aspartate fate (Figure S5B).

To begin testing NEAA synthesis path, we first checked mRNA expressions of amino acid metabolism enzymes in low glutamine. Expectedly, glutamine starvation (0.1mM) alters expression of many transaminases coupled with Atf4 induction, a component of amino acid starvation response (Figure S5C). Interestingly, however, genes that would use aspartate in the cytosol (Got1 and Asns), but not in the mitochondria (Got2) is upregulated in low glutamine (Figure S5C). This also appears more generalizable with other transaminase that cytosolic isoforms are often upregulated while mitochondrial isoforms remain unchanged or down-regulated (Figure S5C). This suggested cytosolic transaminations, or specifically cytosolic aspartate contribution to NEAA synthesis could be more important under glutamine limitations. In fact, levels of many NEAAs are reduced in AGC1-KD cells upon CB-839 treatment or in low glutamine and this is partially rescued by aspartate supplementation (Figure 6B). However, these observations alone do not particularly prove NEAAs being limiting in low glutamine. In addition, because transamination reactions are highly reversible and conversion of one amino

acid to the other is not uni-directional, NEAAs might also be consumed to make aspartate when aspartate levels drop upon glutamine withdrawal.

Therefore we examined this path further using a different approach. To test whether aspartate or other NEAAs are the necessary products of transaminations to rescue cells in glutamine limitations, we provided cells with either mixture of NEAAs or aspartate together with universal transaminase inhibitor aminooxyacetate (AOA) (Figure 6C, S5D). Similar to aspartate, high levels of NEAAs rescue AGC1-KD cells with glutaminase inhibition however this rescue is completely blunted by AOA, suggesting that NEAAs could only rescue glutaminase inhibition through undergoing transaminations (Figure 6D, S5E). Notably, none of the amino acids, including asparagine, can rescue glutaminase inhibitions individually, except for the partial rescue of glutamate, which is itself the product of glutaminase (Figure 6E). On the other hand, AOA treatment reduces the survival of control cells to the level of AGC1-KD cells upon CB-839 treatment (Figure 6D), highlighting that control cells would have no advantage over AGC1-KD cells without aspartate production. Importantly, AOA treatment did not affect proliferation/survival of cells rescued with aspartate, arguing that aspartate does not require to undergo transaminations to rescue glutamine limitations. These data suggest that aspartate is an essential end product of transamination reactions and not particularly limiting for NEAA synthesis when glutamine anaplerosis is inhibited.

In addition to NEAA synthesis, these findings also argue that contribution of aspartate to TCA cycle or cytosolic NAD+ regenerations are also not essential to rescue proliferation/survival as these fates would also begin with a transamination reaction (Figure 6C). Similar to NEAAs, neither da-KG nor pyruvate can completely rescue glutamine limitations when both aspartate aminotransferases are inhibited using AOA or siRNA (Figure 6F-G, S5F), suggesting that conversion of aspartate to oxaloacetate by transamination reactions either to regenerate cytosolic NAD+ or to donate nitrogen is not limiting in AGC1-KD cells upon glutamine-deprivation. It also provides evidence that a major role of anaplerosis is to produce aspartate and TCA cycle activity is not essential for proliferation when exogenous aspartate is provided. Nevertheless, it is important to note these findings do not argue that aspartate does not undergo transaminations and/or fuel TCA cycle, but only suggests that these pathways are not limiting in low glutamine. In fact, we observed that $[U^{13}C]$aspartate incorporates into TCA cycle intermediates in low glutamine (Figure S5G). This is also mirrored in metabolomics experiment where aspartate supplementation modestly increase some of the TCA cycle intermediates (Figure 6B), although these changes are inconsistent across different cell lines or treatments (Figure 6B, S4C-D). Nevertheless, $[U^{13}C]$glutamate tracing data suggest that aspartate is still a relatively weaker fuel for TCA cycle compared to five carbon substrates even when transaminations are active (Figure S5H).

Another downstream path of cytosolic aspartate that is not blocked by AOA is the synthesis of asparagine. Asparagine availability can affect cell survival following glutamine-deprivation (Ratnikov et al., 2015; Zhang et al., 2014), and intracellular asparagine acts as an exchange factor to import other extracellular amino acids when glutamine metabolism is compromised (Krall et al., 2016). Levels of asparagine are also reduced in AGC1-KD cells upon glutamine-starvation and these levels are partially recovered by aspartate supplementation (Figure 6B). However, individual supplementation of asparagine failed to rescue CB-839 treated AGC1-KD cells (Figure 6E) indicating that asparagine production alone does not appear to be limiting for the survival of AGC1-KD cells.

Aspartate is required for proliferation in part because it supports nucleotide biosynthesis (Sullivan et al., 2015). Glutaminase inhibition suppresses pyrimidine biosynthesis in Von Hippel-Lindau (VHL)-deficient renal tumors (Okazaki et al., 2017) suggesting that these perturbations might converge on nucleotide metabolism. When aspartate is used for purine biosynthesis, fumarate is generated as a byproduct (Lane and Fan, 2015). We considered that this may account for the more prominent increase in fumarate levels compared to other TCA cycle intermediates, after aspartate supplementation (Figure 6B). To test whether glutaminase inhibition affect nucleotide biosynthesis rate, we traced [^{15}N-(amide)]glutamine into nucleotides during CB-839 treatment. Because aspartate donates its nitrogen to IMP for AMP production, AMP synthesis from IMP could be impaired when cytosolic aspartate is limiting (Figure S5I). Strikingly, relative AMP/IMP ratio is significantly impaired upon CB-839 treatment and is completely rescued by aspartate supplementation (Figure 6H), arguing aspartate depletion slowed down nucleotide biosynthesis rate. Similarly, intracellular UMP levels are also lower in AGC1-KD cells upon CB-839 compared to controls, suggesting that pyrimidine synthesis pathway is also affected by cytosolic aspartate delivery (Figure 6I). Although it is interesting to note that purine synthesis is much more strongly affected by CB-839 treatment. Nevertheless, these findings argue that glutamine anaplerosis could cause aspartate-dependent defects in nucleotide biosynthesis. As discussed above, the changes in metabolite levels may not sufficiently prove those are limiting in given conditions. To test whether nucleotides were in deed limiting for AGC1-KD cells, we supplemented AGC1-KD and control cells with nucleotide bases. Because aspartate is involved in both purine and pyrimidine synthesis, we supplemented cells with a combination of nucleotide salvage pathway precursors thymine, uridine (for pyrimidines), hypoxanthine, adenine and guanine (Figure S5I). These supplementations improved the proliferation/survival of AGC1-KD cells under low glutamine or glutaminase inhibtions (Figure 6J, S5J), suggesting that nucleotide biosynthesis is one limitation caused by glutamine unavailability. Overall, these data are consistent with cytosolic aspartate preventing cell death and supporting proliferation by preserving nucleotides following glutamine-deprivation.

AGC1 knockdown limits tumor growth and sensitizes tumors to CB-839 treatment

We next examined whether AGC1 knockdown would affect tumor growth *in vivo*. We injected LLC1 cells with or without AGC1-KD into syngeneic C57BL/6 mice and monitored tumor progression. Knockdown of AGC1 slowed tumor growth over the course of 16 days (Figure S6A, B).

Glutaminase inhibitor CB-839 is ineffective in some cancer models *in vivo* even when the cells derived from those tumors are sensitive to CB-839 in culture (Biancur et al., 2017; Davidson et al., 2016). To test whether AGC1-KD sensitizes tumors to CB-839 *in vivo,* we exposed mice with control and AGC1-KD LLC1 tumors to CB-839. CB-839 treatment further reduced the growth of AGC1-KD LLC1 tumors (Figure 7A, S6C) while having a minor effect on control tumors, although causing comparable drops in glutamate/glutamine ratio in both (Figure 7B). Similar to *in vitro* culture, pyruvate/lactate ratio was lower in AGC1-KD tumors, highlighting that loss of AGC1 affects the redox state of the cells (Figure 7C). Interestingly, asparagine levels were increased in CB-839 treated tumors yet were still lower in AGC1-KD tumors compared to controls (Figure 7D, S6D). These findings are consistent with mitochondrial

aspartate export being important when glutamine anaplerosis is inhibited and suggests that the inability to maintain cytosolic aspartate levels slows down growth of AGC1-KD tumors upon CB-839 treatment. Together, these findings argue that AGC1-KD reduces tumor growth and makes tumors vulnerable to glutaminase inhibition *in vivo*.

To test whether AGC1-KD would have similar effects on another type of cancer, we performed allografts with AL1376 pancreas ductal carcinoma cell line derived from a KrasG12D, P53-/- mouse model (Mayers et al., 2014). Consistently, AGC1-KD significantly impaired tumor growth (Figure S6E). In addition, unlike LLC1, AL1376 tumors were completely resistant to CB-839 treatment, yet AGC1-KD improved sensitivity to the drug (Figure S6E-F). These data suggest that targeting AGC1 may synergize with the glutaminase inhibitors to limit growth of some tumors.

To explore the relevance of our findings in human cancer, we investigated tissue microarrays containing several types of human solid tumors using immunohistochemistry with antibodies against AGC1. AGC1 is expressed in several tumors including glioblastoma, as well as adenocarcinoma of ovary and pancreas (Figure S7A, B). While pancreas ductal carcinoma (PDAC) cells have heterogeneous AGC1 expression, all healthy pancreatic duct cells are AGC1-negative, suggesting that AGC1 might be upregulated during tumorigenesis in this cancer type (Figure S7B). Although we did not observe a prominent up-regulation of AGC1 protein in Kras^{G12D}, P53$^{-/-}$ mouse lung (Davidson et al., 2016) or pancreas (Mayers et al., 2014) tumors, both tumor types had abundant AGC1 expressions (Figure S7C). These observations suggest that targeting AGC1 could be relevant for cancer therapy.

DISCUSSION

Our results argue that glutamine anaplerosis is important to produce aspartate and that decreased cytosolic aspartate levels upon glutamine starvation lead to cell death. These findings are consistent with recent data showing AGC1-deficient neuroblastoma cells proliferate slower in low-glutamine media (Profilo et al., 2017). From a mechanistic standpoint, it appears that AGC1 functions to sustain proliferation/survival of glutamine-deprived cells by providing aspartate to the cytosol. While our data argue that aspartate may be more limiting for nucleotide biosynthesis following glutamine depletion, we appreciate that other paths of aspartate could be more limiting in other circumstances. It is also important to recognize that if one fate of aspartate is rescued, then more of this metabolite will be available for other pathways. For these reasons we are hesitant to definitively conclude that nucleotides is the only critical fate of aspartate, particularly as our data suggest that levels of other non-essential amino acids or TCA cycle intermediates are indirectly affected when cytosolic aspartate is depleted. Furthermore, it is impossible to rescue aspartate use for protein synthesis in the same way that aspartate use for nucleotides can be rescued by providing exogenous bases. Furthermore, in C2C12 cells, AGC1 is the predominant isoform over AGC2 that is structurally and functionally similar (Thangaratnarajah et al., 2014). While we focused here on the AGC1 isoform, we speculate that complete loss of both isoforms could cause superior limitations and significantly impair cell survival, perhaps even under glutamine-replete conditions. Similarly, AGC2 depletion could be more harmful for some cell types than AGC1 depletion.

Glutamine metabolism in cancer can be influenced by the environment (Davidson et al., 2016). For instance, extra physiological cystine levels in tissue culture media can promote both glutaminase activity and glutamine-dependency (Muir et al., 2017). Consistent with these findings, glutamine contributes very little to the oxidative TCA cycle in some cancers *in vivo*, where reductive glutamine metabolism is more prominent (Davidson et al., 2016). Similar to high-cystine conditions, increased mitochondrial NAD+/NADH ratio could also enhance oxidative glutamine metabolism and drive glutamine flux into aspartate synthesis. We observed that AGC1-KD suppressed reductive glutamine metabolism in C2C12 cells, and this may also be the case for LLC1 cells *in vivo*, potentially explaining why AGC1-KD tumors became sensitive to glutaminase inhibition *in vivo*.

There are three glutaminase isoforms in mammalian cells: liver isoform (LGA), kidney isoform (KGA) and a splice variant of KGA (GAC, also known as glutaminase C) that localizes to mitochondria (Cassago et al., 2012). GAC is the enzymatically most efficient isoform and is often upregulated in cancers, and connected to glutamine anaplerosis (Cassago et al., 2012). Upon CB-839 treatment, which selectively inhibits GAC (Gross et al., 2014), cells may utilize cytosolic glutamate as an alternative source. Because AGC1 exports aspartate from mitochondria in exchange of cytosolic glutamate, decreased glutamate delivery to mitochondria might also contribute to CB-839 toxicity in AGC1-KD cells. However, considering that there are two other glutamate importers located in the inner mitochondrial membrane, Slc25a22 and Slc25a18, (Palmieri, 2013) we lack evidence to speculate that mitochondrial glutamate uptake is limiting for AGC1-KD cells. However, if mitochondrial glutamate uptake would be limiting, glutamate supplementation should rescue control, but not AGC1-KD cells. Because glutamate

rescued both control and AGC1-KD cells similarly, we speculate that impaired glutamate entry to mitochondria is not the primary cause of cell death. On the other hand, inability of alpha-ketoglutarate to fully rescue glutamine limitation when aspartate synthesis is blocked suggests that a potential deficiency in mitochondrial glutamate uptake could be a factor that exacerbates the drop in mitochondrial aspartate levels in AGC1-KD cells, but not the sole cause of impaired proliferation or cell death. Instead, our data are more consistent with cytosolic glutamate supporting survival via a pathway independent from cytosolic aspartate delivery.

Although usually lead to similar phenotypes, we appreciate the variability between low-glutamine and CB-839 treatments. Because low glutamine will affect more pathways than CB-839 treatment, cell proliferation/survival phenotypes and the depletion of some non-essential amino acids and TCA intermediates were sometimes stronger in low glutamine compared to CB-839 treatment. To minimize the possibility that glutamine becomes limiting for pathways other than glutamine anaplerosis, we avoided completely removing glutamine from the media. However, lowering glutamine concentration does not necessarily divert glutamine from anaplerosis or does not prove that it will never be limiting for its other fates such as nucleotide or amino acid biosynthesis. Therefore, using the glutaminase inhibitor is more informative tool to narrow down the fate of glutamine that is required for proliferation/survival of AGC1-KD cells. As CB-839 synergizes with AGC1-KD similarly to low glutamine, we concluded that main reason why AGC1-KD cells are sensitive to glutamine withdrawal was the anaplerosis function of glutamine.

Mitochondrial transporters are not always specific to certain substrates and could transport several additional metabolites across membranes with varying binding efficiencies. For instance, uncoupling protein 2 (UCP2) was shown to export four carbon metabolites from mitochondria, including aspartate. We speculate that unspecific mitochondrial transporters maintains some degree of cytosolic aspartate delivery in AGC1-KD cells as long as there is high enough aspartate in mitochondria, for instance when TCA cycle is fed. However, these transporters may not be able to recognize aspartate when it is at too low levels, making specific aspartate transporter AGC1 more crucial for cytosolic aspartate delivery. Apart from unspecific transporters, it also likely that AGC2 function alone is not sufficient when mitochondrial aspartate levels are too low. Therefore, AGC1-KD cells depend on anaplerosis substrates to maintain proliferation/survival significantly more than control cells. Interestingly however, not all anaplerosis substrates tested could rescue AGC1-KD cells under glutamine limitations. Unlike pyruvate or daKG, dimethlymalate (dMal, cell permeable form of malate) (, (Heart 2009) supplementation failed to rescue low glutamine or CB-839 treatment (Figure S4A-B) and was more harmful than CB-839 treatment alone on some cells (data not shown). In addition, dMal was not sufficient to boost aspartate levels, unlike other anaplerosis sources (Figure S4C-D) even induced a reduction in TCA intermediates in some conditions. These data suggest that dMal might have potentially harmful off-target effects on the cells other than solely supplying four carbon units to TCA cycle. In theory, increasing cytosolic malate levels might disrupt canonical malic enzyme pathway or malate-aspartate shuttle. Furthermore, several mitochondrial transporters use malate as an exchange factor including one citrate, a-KG and phosphate transporters (Palmieri, 2013). Therefore it is possible that importing excess amounts of malate into mitochondria may cause a carbon or energy deficiency for mitochondria that

negates a potential contribution from malate anaplerosis. Collectively, these points might explain why dMal fails to rescue glutamine limitations unlike other anaplerosis substrates.

We used asparagine levels as a proxy for cytosolic aspartate; however mouse plasma contains asparagine (Rivera et al., 1987) and this may explain why we did not observe any differences in asparagine levels in AGC1-KD tumors compared to controls *in vivo.* Interestingly, asparagine levels were increased with CB-839 treatment *in vivo* independently of AGC1 expression*,* in line with recent reports pointing out that asparagine synthase expression is upregulated in CB-839-resistant cells (Biancur et al., 2017)*.* This may suggest an independent, anti-apoptotic function for asparagine as previously reported (Zhang et al., 2014). In our system, asparagine supplementation had no effect on CB-839 treated cells *in vitro*, however this may change when cells are adapted to grow in the presence of glutaminase inhibitors (Krall et al., 2016). Alternatively, asparagine levels might be elevated to sustain glutamate levels via asparagine synthetase activity. In addition, because asparagine is produced from both cytosolic aspartate and glutamine, in a media condition where glutamine is limited, asparagine levels alone cannot be used as proxy for cytosolic aspartate. This may explain why aspartate supplementation (or other anaplerosis sources) did not increase asparagine levels under low glutamine as they did upon CB-839 treatment (Figure 6D).

Aspartate availability may be limiting for tumor growth *in vivo* (Gui et al., 2016) and we find that AGC1-deficiency leads to both reduced cytosolic aspartate and increased dependence on glutaminase. These findings suggest that combination therapies targeting both aspartate and glutamine metabolism may be synergistic. We found that AGC1 plays a central role in sustaining cytosolic aspartate levels, particularly when mitochondrial glutaminolysis is compromised. This implies that targeting AGC1 could sensitize cancers to glutaminase inhibitors. It is worth noting that genetic background and tissue of origin are also important aspects to consider for targeting metabolism (Mayers et al., 2016; Yuneva et al., 2012), and additional studies are necessary to define the cancer subsets that are most likely to respond to these interventions. Furthermore, potential toxicities of AGC inhibition in healthy cells should also be held in caution as several diseases were reported concerning loss of either AGC isoforms. AGC1 deficiency in mice and humans leads to loss of motor coordination and neuronal defects (Falk et al., 2014; Jalil et al., 2005; Sakurai et al., 2010; Wibom et al., 2009), while loss-of-function mutations in AGC2 leads to the urea cycle-associated disorder type II-citrullinemia (Saheki et al., 2002; Yasuda et al., 2000). Nevertheless, our data provide evidence that tumor-specific inhibition of AGC1 significantly reduces tumor growth and this effect could be exacerbated with glutaminase inhibitor.
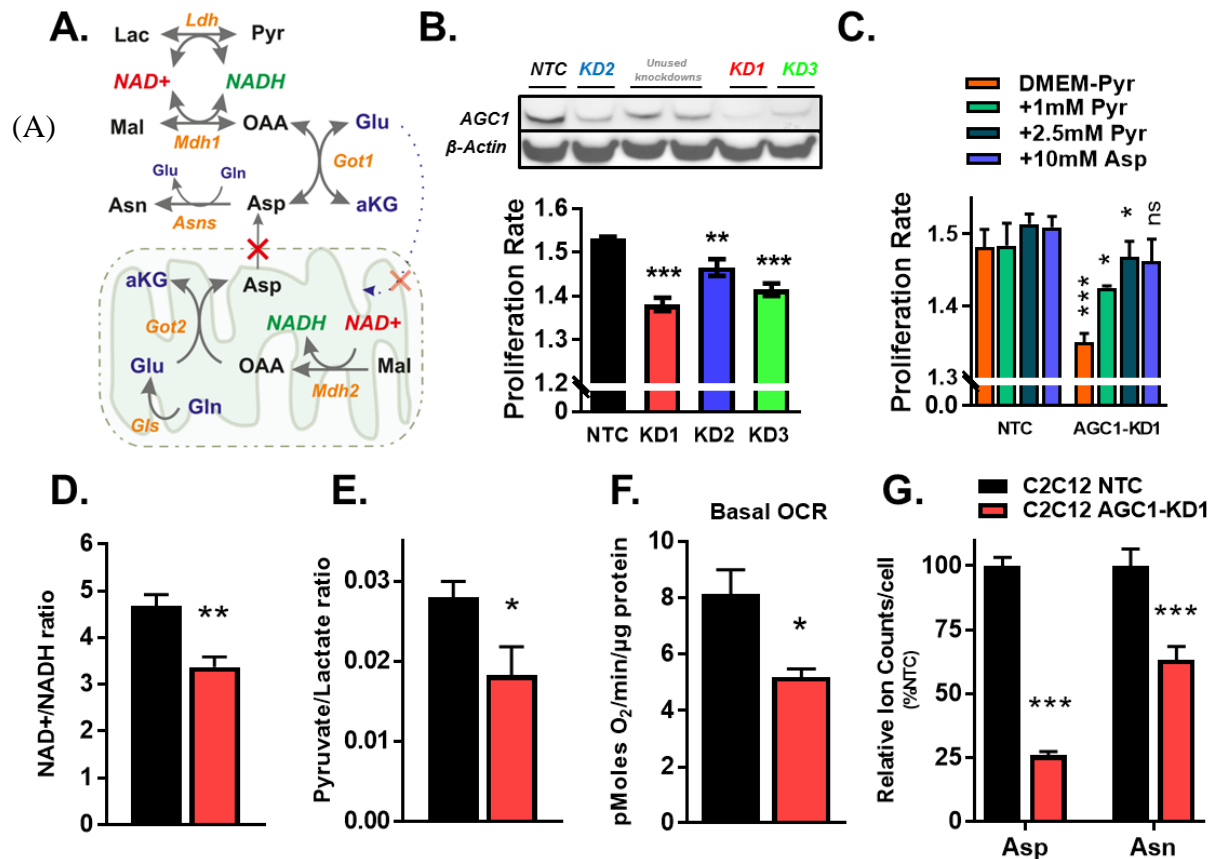
ACKNOWLEDGEMENTS

FIGURES

Figure 1. Knockdown of AGC1 decrease cytosolic aspartate levels and increase dependency for exogenous electron acceptors

Figure 1 Legends: (A) Aspartate regenerates NAD+ in the cytosol through consecutive glutamate-oxaloacetate dehydrogenase (Got1) and malate dehydrogenase (Mdh1) reaction as part of the malate-aspartate shuttle. (B) 3 out of 5 shRNA substantially knocked-down AGC1 (above). Proliferation rate of AGC1 knockdown cells were determined using cell viability assay. Fold change of viable cell number was used for determining number of cell division and presented as doublings/day (n=3) (below). (C)　Proliferation rate was determined in the presence and absence of pyruvate and aspartate. Final cell counts were normalized to cell number before media conditions were applied (n=3). (D) Intracellular NAD+/NADH ratio was determined in pyruvate free DMEM using luminometric assay (n=5), Mean ± SEMs are shown. (E) Pyruvate to lactate ratio was determined from cells grown in pyruvate-free media using GCMS (n=3). (F) Basal oxygen consumption rate was assessed using Seahorse XF96 in serum-free, phenol-red free media containing 5mM Glucose, 1mM sodium pyruvate and 2mM glutamine (n=3, each including 7-8 technical replicates). (G) Cellular aspartate and asparagine levels in standard DMEM conditions excluding pyruvate are measured using GCMS analysis (n=3).

All figures denote mean ± SD unless indicated otherwise. * $p \leq 0.05$, ** $p \leq 0.01$, *** $p \leq 0.001$. See also (Figures S1)

**Figure 2. AGC1-KD cells are sensitive to glutamine withdrawal**
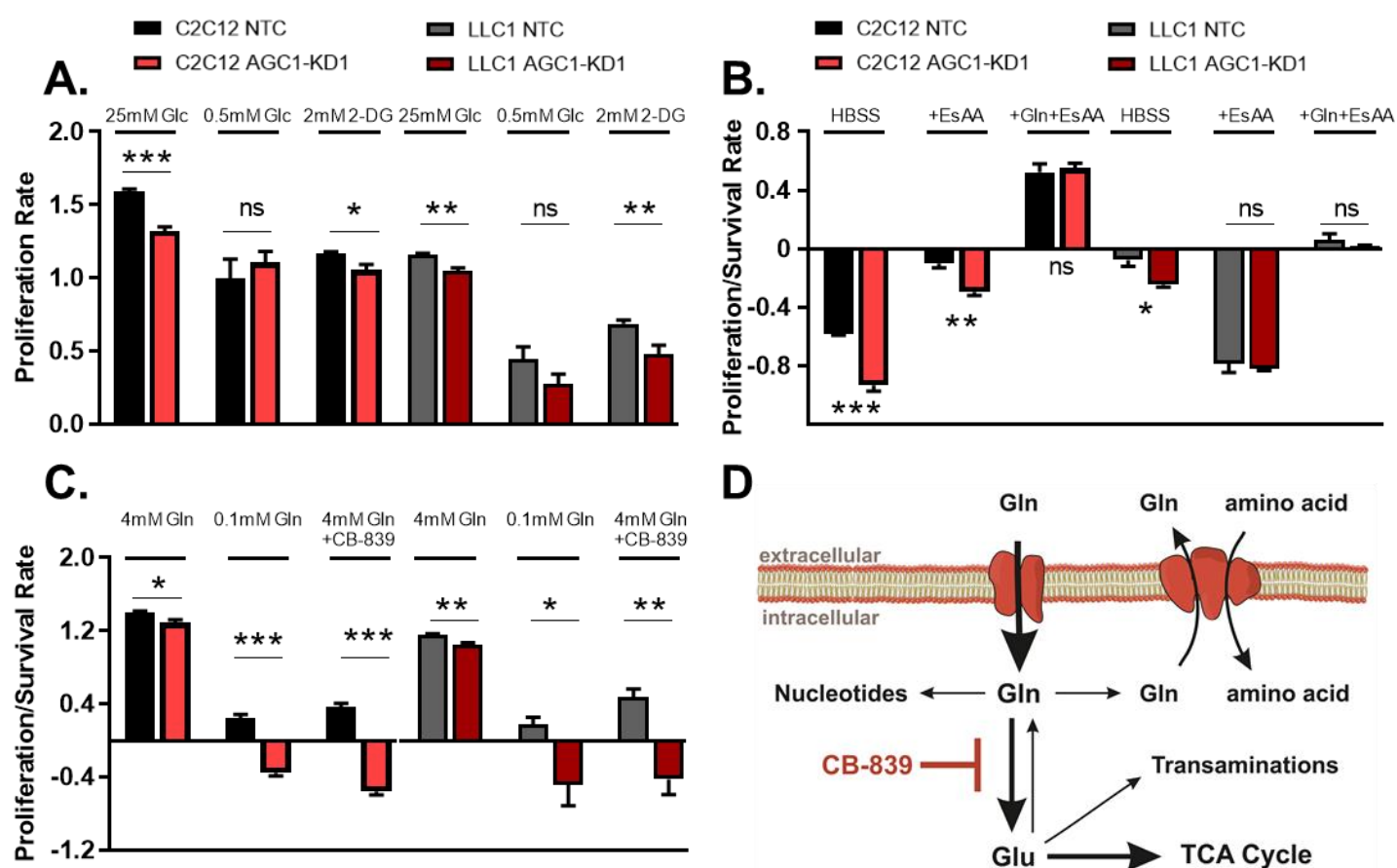
Figure 2 Legends: (A) Proliferation rate was determined using cell viability assay in pyruvate-free DMEM containing initial concentrations of 25mM or 0.5mM glucose (Glc) or 25mM glucose supplemented with 2mM 2-deoxyglucose (2-DG) (n=5). (B)Survival rate of the cells with or without essential amino acids (EsAA) and glutamine (Gln) was measured using cell viability assay in amino acid-free, pyruvate-free HBSS containing 5mM glucose supplemented with 10% FBS, and vitamins (n=3). (C) Proliferation/survival rate was assessed using cell viability assay in pyruvate-free DMEM containing initial concentrations of 4mM or 0.1mM glutamine or 4mM supplemented with 1μM glutaminase inhibitor CB-839 (n=5). (D) Schematic overview of glutamine's potential fates within a cell.

All figures represent mean ± SEM unless indicated otherwise.

* $p \leq 0.05$, ** $p \leq 0.01$, *** $p \leq 0.001$.

See also (Figures S1)

Figure S1. AGC1 overexpression increases proliferation, NAD+/NADH ratio and aspartate levels, opposite to AGC1 knockdown
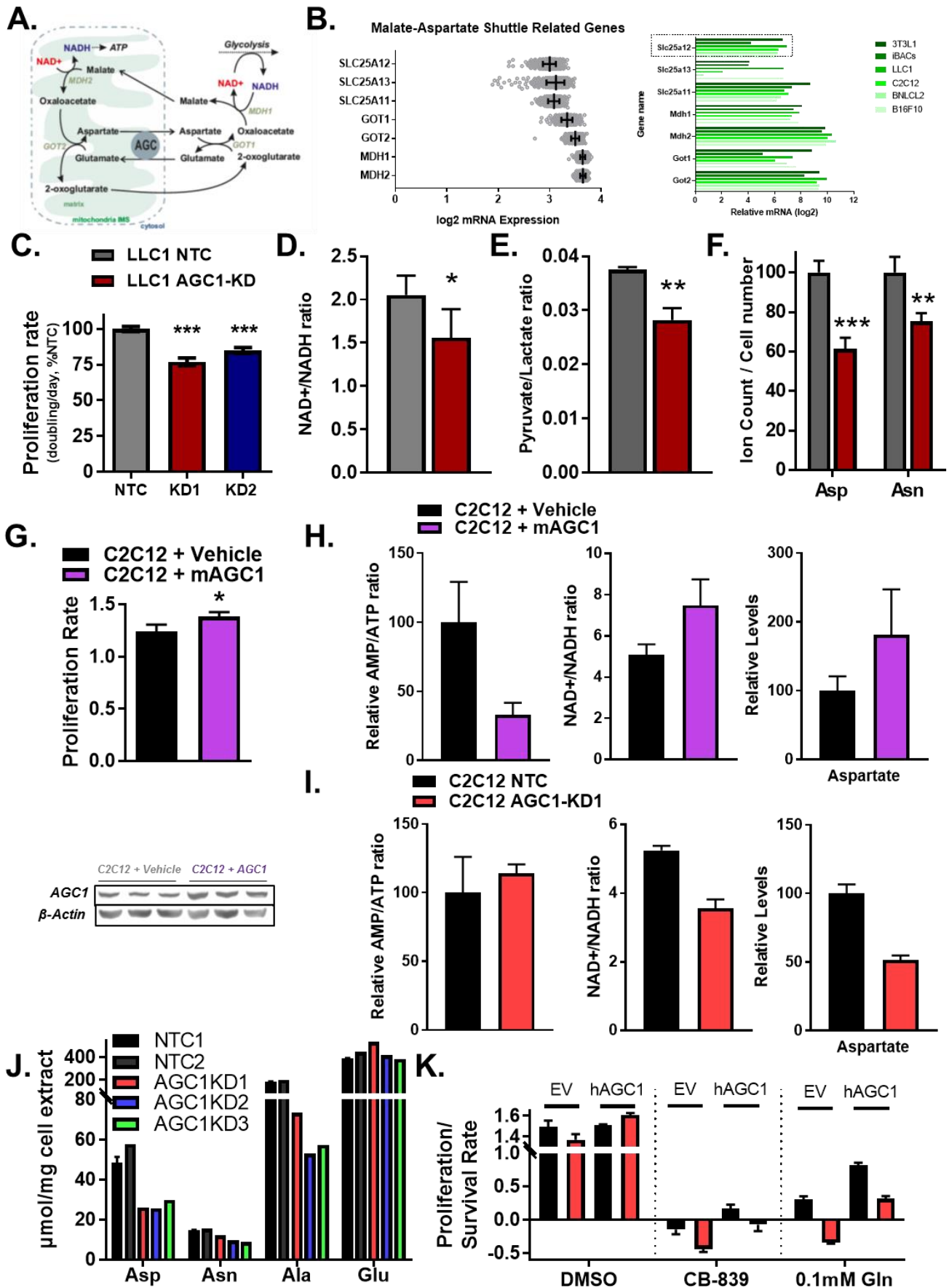
Figure S1 Legends: (A) Schematic overview of canonical Malate-Aspartate Shuttle (MAS). (B) mRNA expressions of MAS components in [left] human cell lines adopted from Cancer Cell Line Encyclopaedia (CCLE) or [right] in transformed or non-transformed mouse cell lines in proliferating stage determined using qPCR (compared to TfIIb housekeeping gene) (n=1). (C) Proliferation rate of AGC1 knockdown LLC1 cells was determined using cell viability assay. Fold change of viable cell number was used for determining number of cell division and proliferation rate is presented as percent of control cells (n=3) (D) Intracellular NAD+/NADH ratio was determined in pyruvate free DMEM (n=5) Mean ± SEMs are shown. (E) Pyruvate to lactate ratio was determined from cells grown in pyruvate-free media using GCMS (n=3). (F) Cellular aspartate and asparagine levels in standard DMEM conditions excluding pyruvate are measured using GCMS analysis (n=3). (G) (Above) Proliferation rate of AGC1 overexpressing C2C12 cells was determined in the absence of pyruvate. Final cell counts were normalized to initial cell number before transfection occurred (n=3). Paired ttest was used to make comparison between groups. (Below) AGC1 protein expressions of C2C12 cells after the proliferation assay. (H-I) AMP/ATP ratio, NAD+/NADH ratio and Aspartate levels were measured in C2C12 cells that (H) transiently overexpressed mouse AGC1 or (I) that had stable knockdown of AGC1. (J) Aspartate, asparagine, alanine, and glutamate levels in C2C12 cells that individually express 2 independent non-targeting shRNA controls (NTC1 and NTC2) or 3 independent shRNAs targeting AGC1 (KD1, KD2 or KD3). n=2 for NTC1, n=1 for the subsequent groups. (K) Proliferation/survival rate of AGC1 knockdown cells, transfected with empty vector (EV) or with human AGC1 (hAGC1) were determined using cell viability assay. Media conditions were applied approximately 20 hours after transfection and fold change of viable cell number was determined two days after incubation. (n=3) mean ± SD are shown.

All figures denote mean ± SD unless indicated otherwise. * $p \leq 0.05$, ** $p \leq 0.01$, *** $p \leq 0.001$.

Figure 3. AGC1-KD cells show increased oxidative TCA cycling
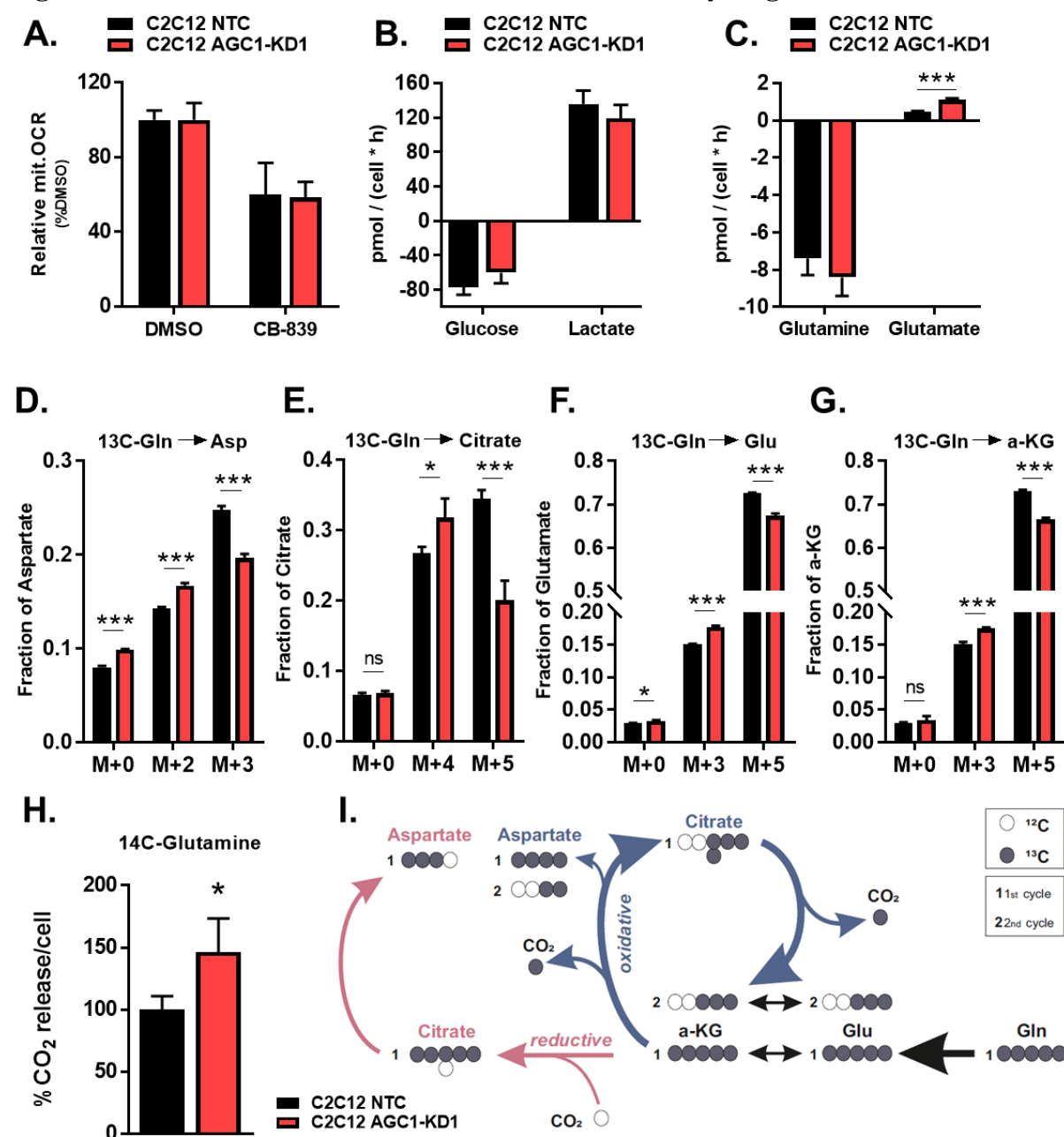
Figure 3 Legeneds: (A) Basal oxygen consumption rate in the presence and absence of CB-839 was determined using Seahorse XF24 (n=5), mean ± SEMs are shown. (B-C) Changes in glucose, lactate, glutamine, and glutamate concentrations in the media for 48h was measured using metabolic flux analyzer YSI and normalized to area under the growth curve for uptake rate calculations (n=3). (D-G) [U13C]glutamine (Gln) tracing into aspartate (Asp), citrate, glutamate (Glu) and alpha-ketoglutarate (α-KG) after 24hours was determined using GCMS analysis (n=3). (H) Radioactive CO_2 release from C2C12 cells was measured 1 hour after 14C-Glutamine treatment (n=3). (I) Schematic overview of oxidative and reductive glutamine catabolism. Oxidative demonstrate higher M+3/M+5 ratio of Glu and α-KG and reduced M+3 and M+5 Asp and citrate, respectively. All figures show mean ± SD unless indicated otherwise. * $p \leq 0.05$, ** $p \leq 0.01$, *** $p \leq 0.001$.

See also (Figures S2)

Figure S2. Glucose and glutamine utilization is not drastically altered in AGC1-KD cells
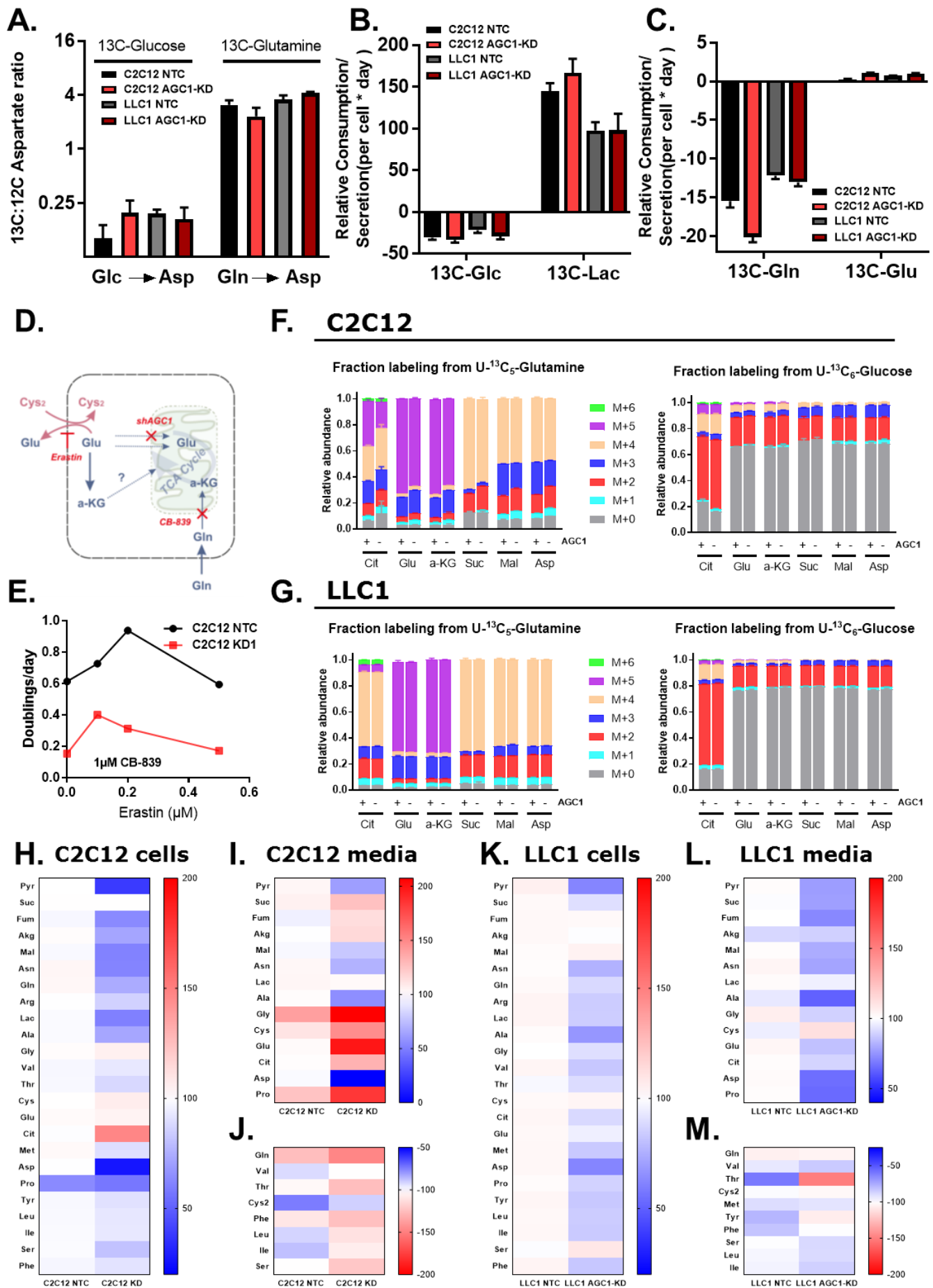
Figure S2 Legeneds: (A) Relative labelled(13C)/unlabeled(12C) aspartate ratio of C2C12 and LLC1 cells incubated with 5mM [U13C]glucose or 2mM [U13C]glutamine in DMEM-Pyr for 12 hours, determined by NMR spectroscopy (n=5). (B) Labelled glucose uptake and lactate release by C2C12 and LLC1 cells in 12 hours, determined by NMR spectroscopy (n=5). (C) Labelled glutamine uptake and glutamate release by C2C12 and LLC1 cells in 12 hours, determined by NMR spectroscopy (n=5). (D) Schematic overview of how Erastin inhibits glutamate export. (E) Proliferation rate of C2C12 cells cultured in 1µM CB-839 and with varying concentrations of Erastin (n=1). (F-G) Steady state (24h) [U13C]glutamine and [U13C]glucose contribution into aspartate (Asp), citrate, glutamate (Glu), alpha-ketoglutarate (a-KG), malate (Mal), and succinate (Suc) in (F) C2C12 or (G) LLC1 cells (n=3). (H, K) Relative total pool sizes of various metabolites in (H) C2C12 and (K) LLC1 cells when cultured in full DMEM-Pyr media for 24h, normalized to cell number; percent change compared to NTC (n=3), medians are shown. (I, L) Relative metabolite secretion by (I) C2C12 and (L) LLC1 cells within 24 hours when cultured in full DMEM-Pyr media, normalized to cell number; percent change compared to NTC (n=3), medians are shown. (J, M) Relative metabolites taken up by (J) C2C12 and (M) LLC1 cells from full DMEM-Pyr media within 24 hours, normalized to cell number; percent change compared to NTC (n=3), medians are shown.

All figures denote mean ± SEM unless indicated otherwise.

**Figure 4. Cytosolic aspartate delivery improves proliferation/survival under glutamine limitations**
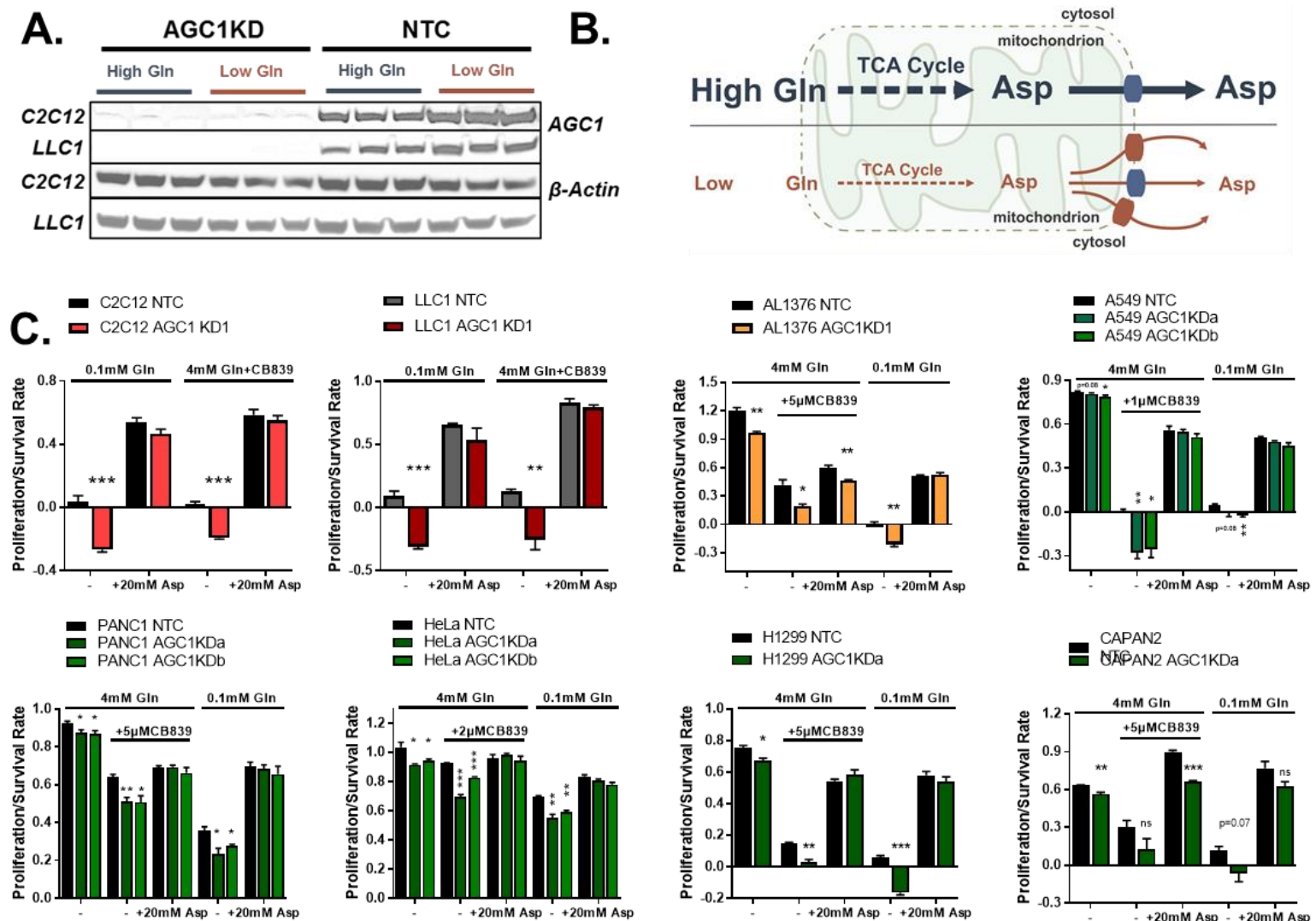
Figure 4 Legends: (A) Western blot images demonstrating AGC1 protein amounts in C2C12 and LLC1 whole cell lysates (40µg/lane) in the presence and absence of 4mM glutamine, 24h post-starvation. (B) High aspartate production suffice to feed cytosolic aspartate demands in the presence of high glutamine. Glutamine starvation causes to a drop in mitochondrial aspartate levels leading to low cytosolic aspartate delivery and increased amount of AGC1 protein. (C) Survival/proliferation rate in pyruvate-free DMEM containing 0.1mM glutamine or CB-839 in the presence and absence of 20mM aspartate determined by cell counting assay (n=3), mean ± SEM.

* p ≤ 0.05, ** p ≤ 0.01, *** p ≤ 0.001.

See also (Figure S3)

# Figure S3. Cytosolic aspartate delivery improves proliferation/survival under glutamine limitations
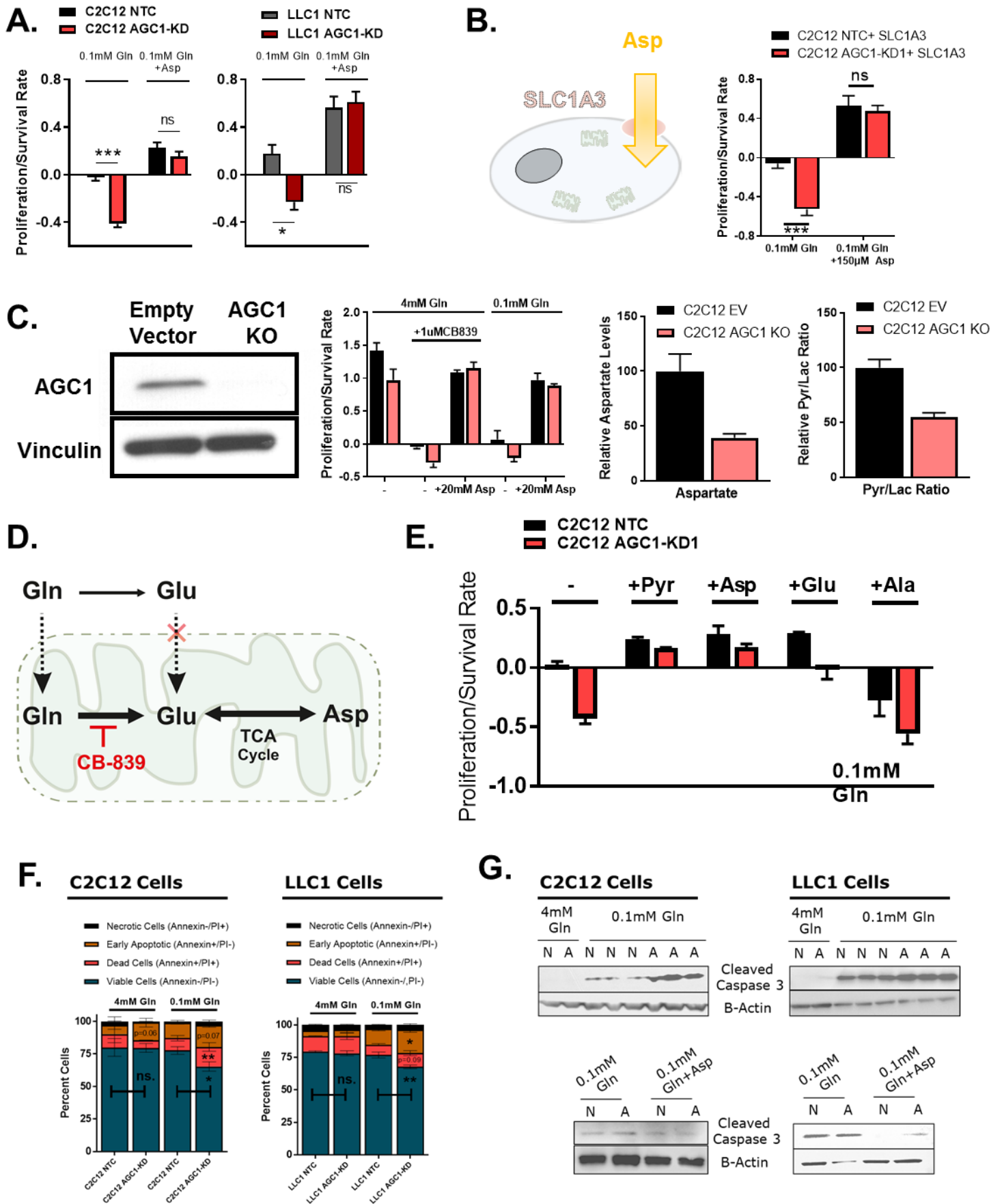
Figure S3 Legends: (A) Survival/proliferation rate in pyruvate-free DMEM containing 0.1mM glutamine in the presence and absence of 5mM aspartate determined by cell viability assay (n=3), mean ± SEM. (B) Survival/proliferation rate of C2C12 cells expressing plasma membrane aspartate transporter SLC1A3 cultured pyruvate-free DMEM containing 0.1mM glutamine in the presence and absence of 0.15mM aspartate determined by cell counting assays (n=3). (C) AGC1 protein amount, survival/proliferation rate, GCMS-measured aspartate levels and pyruvate to lactate ratio of C2C12 cells with CRISPR/Cas9-mediated AGC1 deletion (n=3). (D) Schematic comparison of cytosolic vs mitochondrial glutamate production. (E) Survival/proliferation rate of C2C12 cells cultured in pyruvate-free DMEM containing 0.1mM glutamine in the presence and absence of 5mM glutamate, 5mM aspartate, 2.5mM alanine or 2.5mM sodium pyruvate (n=3). (F) Annexin V and/or propidium iodide (PI) positive C2C12 and LLC1 cells cultured for 24h in the presence and absence of 4mM glutamine, determined by flow cytometry (n=3). (G) Cleaved Caspase 3 protein expression in C2C12 and LLC1 cells cultured for 24h in the presence and absence of 4mM glutamine or 10mM aspartate (n=3).

All figures denote mean ± SDs unless indicated otherwise.

Figure 5. Sustaining cytosolic aspartate levels prevents cell death upon glutamine starvation and glutaminase inhibiton
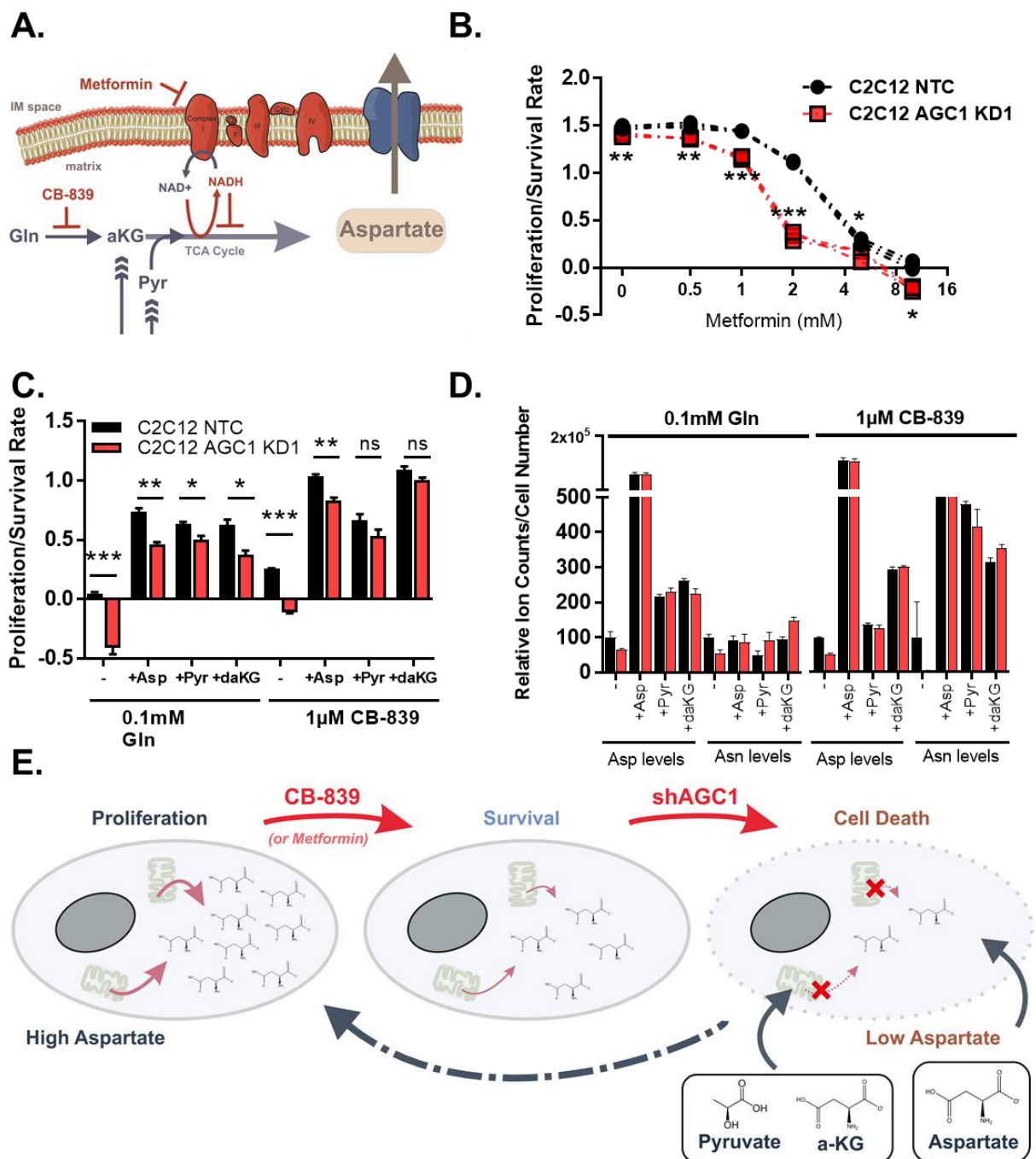
Figure 5 Legends: (A) Glutamine is the major carbon source that supports TCA cycle and aspartate biosynthesis. Pyruvate or aKG could sustain TCA and aspartate production in the absence of glutaminase activity (CB-839 treatment), boosting mitochondria-to-cytosol aspartate efflux. Metformin on the other hand, could block respiration, reducing NAD+/NADH ratio and aspartate synthesis, impairing aspartate efflux. (B) Proliferation/survival rate of C2C12 cells treated with varying concentration of metformin in pyruvate-free DMEM (n=3). (C) Proliferation/survival rate of C2C12 cells treated with low-glutamine (0.1 mM) or 1µM CB-839 in the presence and absence of 20mM aspartate, 2mM sodium pyruvate (pyr), dimethyl-α-ketoglutarate (da-KG) was determined using cell counts. Final cell counts were normalized to cell number before media conditions were employed (n=3). (D) Aspartate and asparagine

levels in low-glutamine or CB-839 treated C2C12 cells in the presence and absence of 20mM aspartate (Asp), 2mM sodium pyruvate (Pyr) and 2mM dimethylalpha-ketoglutarate (daKG). Relative ion counts/cell number normalized to control cells for each treatment (n=3). (E) Schematic representation of the correlation between cytosolic aspartate levels and cell survival. CB-839 (or metformin) reduces cytosolic aspartate levels by blocking glutamine anaplerosis, which is further inhibited by AGC1 knockdown. Pyruvate or aKG restores viability by supporting aspartate synthesis.

All figures denote mean ± SEMs unless indicated otherwise.

* $p \leq 0.05$, ** $p \leq 0.01$, *** $p \leq 0.001$.

See also (Figure S4)

Figure S4. Levels of TCA metabolites and non-essential amino acids
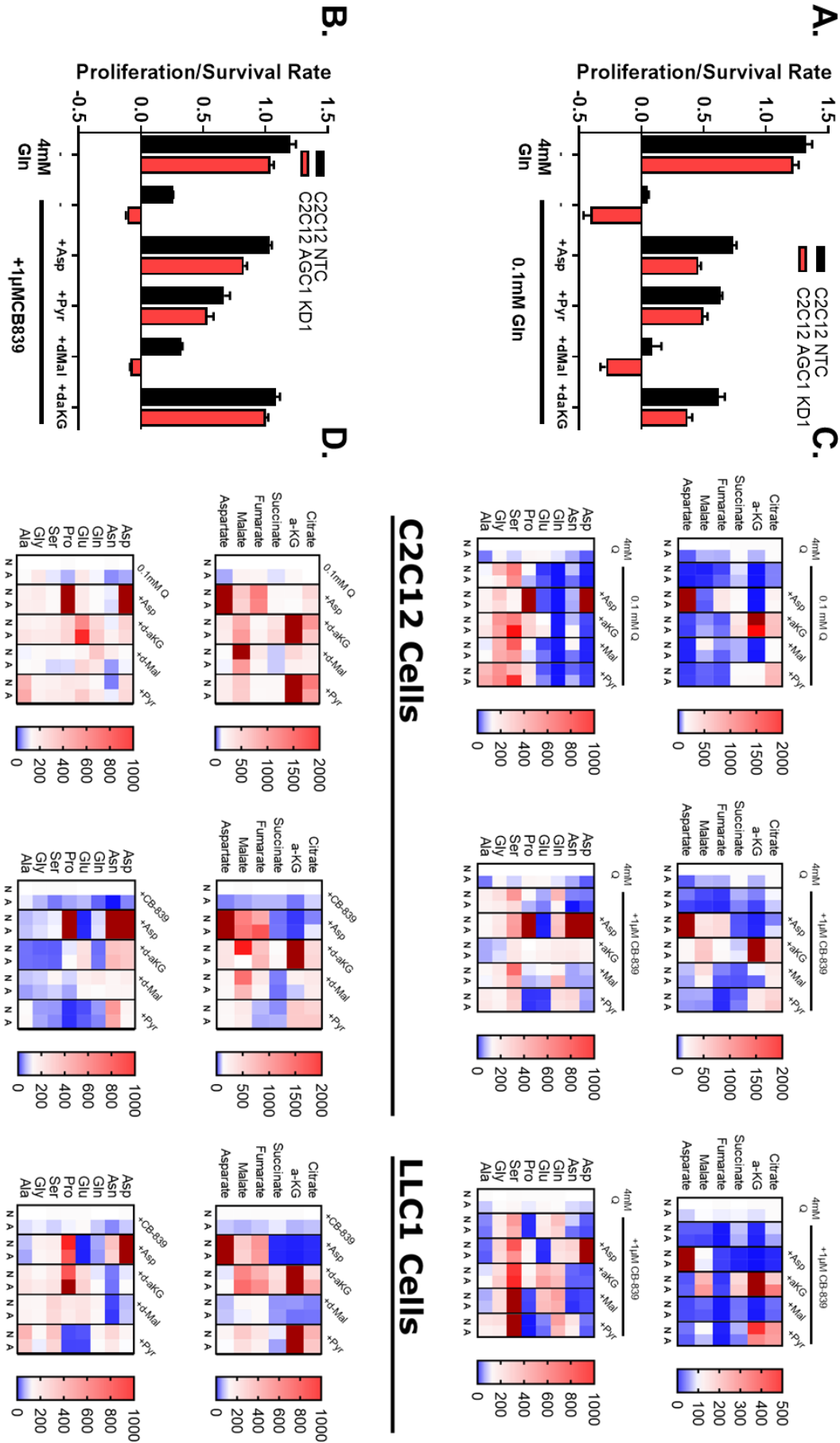
Figure S4 Legends: (A/B) Survival/proliferation rate of C2C12 cells cultured in pyruvate-free DMEM containing 0.1mM glutamine (A) or 1µM CB-839 (B) in the presence and absence of 20mM aspartate, 2mM sodium pyruvate, 2mM dimethylmalate, 2mM dimethylaKG, determined by cell counts (n=3) (C) GCMS analysis of TCA cycle intermediates and non-essential amino acids (normalized to cell number) from cells cultured with 0.1mM glutamine or with 1µM CB-839 for 24h in the presence and absence of 20mM aspartate, 2mM dimethylaKG, 2mM dimethlymalate, or 2mM sodium pyruvate. Percent change compared to NTC+4mM Gln (n=3, means are shown). (D) GCMS analysis of TCA cycle intermediates and non-essential amino acids (normalized to cell number) from cells cultured with 0.1mM glutamine or with 1µM CB-839 for 24h in the presence and absence of 20mM aspartate, 2mM dimethylaKG, 2mM dimethlymalate, or 2mM sodium pyruvate. Percent change compared to NTC+0.1mM glutamine or +1µM CB-839 (n=3, means are shown).

Figure 6. Cytosolic aspartate is limiting for nucleotide biosynthesis under glutaminase inhibition
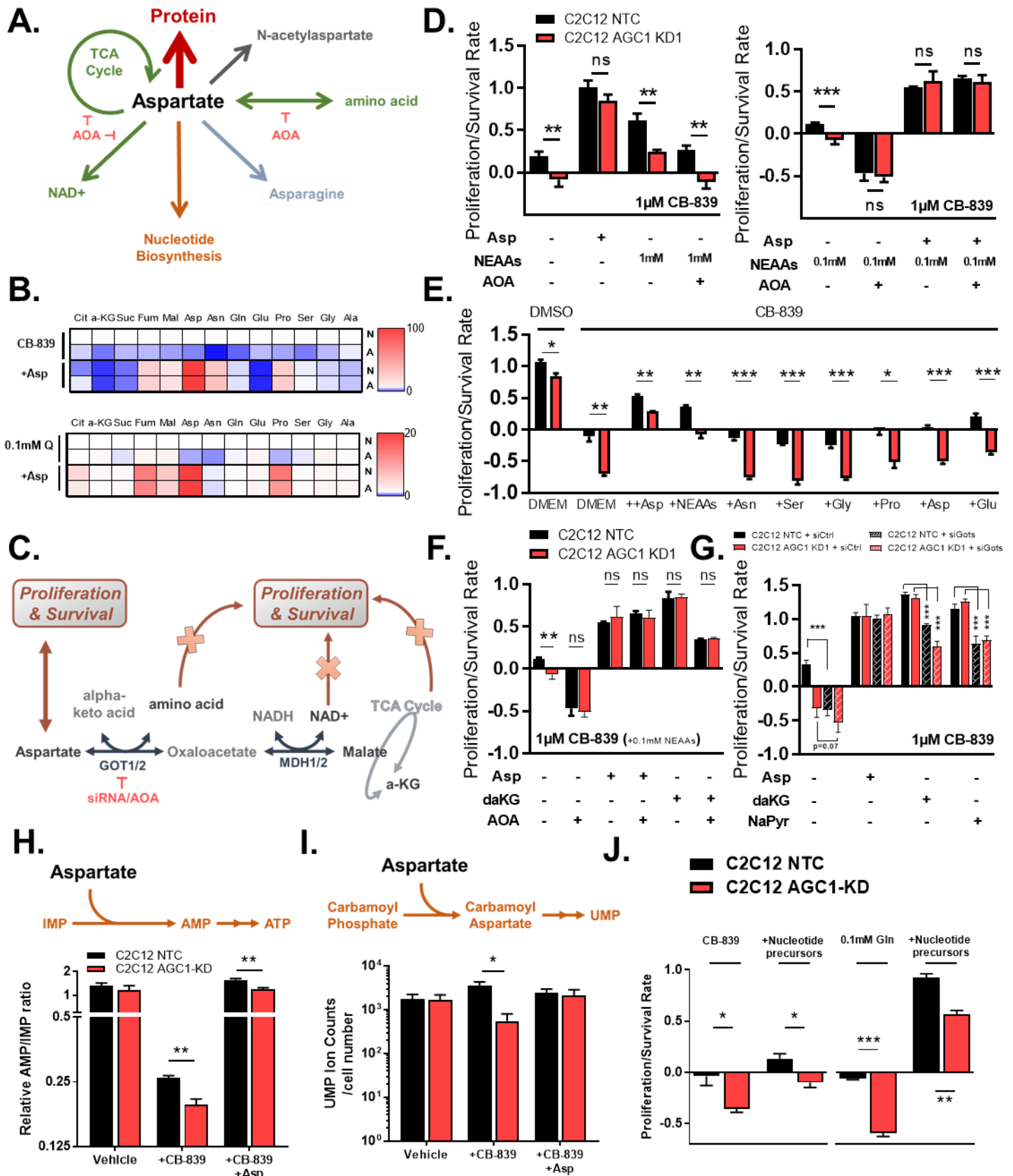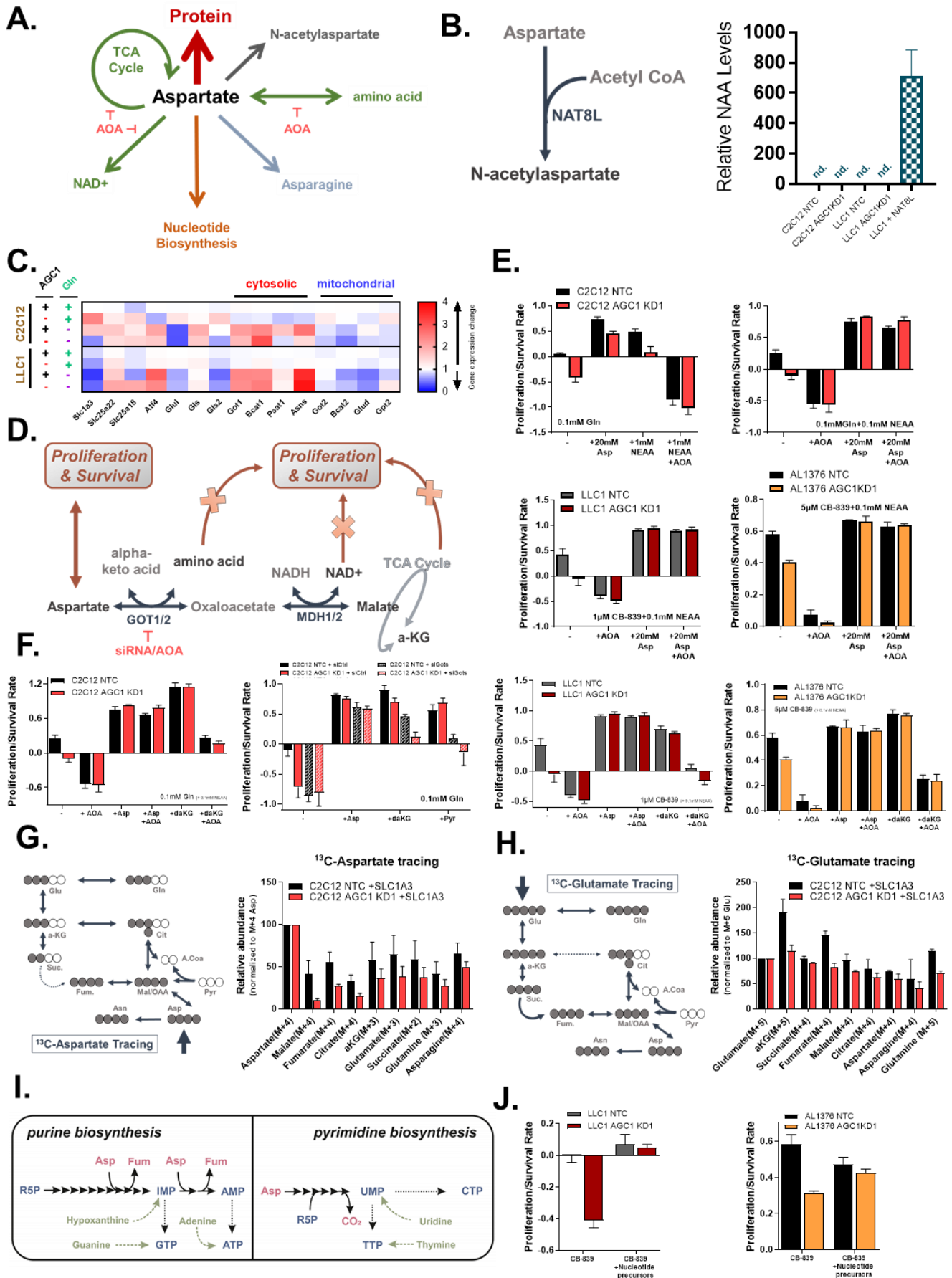
Figure 6 Legends: (A) Schematic overview of potential fates of cytosolic aspartate. Aspartate is a proteinogenic amino acid (red) that could aspartate undergo transaminations (green) to support non-essential amino acid biosynthesis, oxidize cytosolic NADH through malate-aspartate shuttle and recycle back to mitochondria to fuel TCA cycle. 5) Asns enzyme produces asparagine in the cytosol (blue) consuming aspartate, glutamine and ATP. 6) Aspartate is acetylated to make N-acetylaspartate (gray). 7) Aspartate is an essential component of purine and pyrimidine biosynthesis (orange). (B) GCMS analysis of non-essential amino acids and TCA cycle intermediates (normalized to cell number) from C2C12 cells treated with CB-839 or low-glutamine (0.1mM Q) for 24h in the presence and absence of 20mM aspartate, percent change compared to NTC with CB-839 or NTC with 0.1mM Q (n=3, means were shown) (C) Aspartate undergoes transaminations (Got1/2) to support amino acid biosynthesis, TCA cycle and NADH oxidation. TCA substrates or amino acids also undergo transaminations to produce aspartate. Experiments with using AOA or siGot1/2 may underlie which end product is most limiting. (D) Proliferation/survival rates of C2C12 cells treated with 1μM CB-839 in the presence and absence of 20mM aspartate, 1mM or 0.1mM of a mixture of non-essential amino acids containing serine, glycine, alanine, aspartate, asparagine, proline, and glutamate or 0.3mM AOA (n=3). (E) Proliferation/survival rates of C2C12 cells treated with 1μM CB-839 in the presence and absence of 10mM aspartate, 1mM of a mixture of non-essential amino acids containing serine, glycine, alanine, aspartate, asparagine, proline, and glutamate or 1mM of indicated free amino acid (n=3). (F) Proliferation/survival rates of C2C12 cells treated with 1μM CB-839 in the presence and absence of 20mM aspartate, 2mM dimethylalpha-ketoglutarate (d-aKG), or 0.3mM AOA (n=3). (G) Proliferation/survival rates of C2C12 cells treated with 1μM CB-839 in the presence and absence of 20mM aspartate, 2mM dimethylalpha-ketoglutarate (d-aKG), 2mM sodium pyruvate (NaPyr) or siRNA targeting Got1 and Got2 (n=3). (H) LCMS analysis of relative AMP to IMP ratio in C2C12 cells treated with CB-839 for 24h in the presence and absence of 20mM aspartate, (n=3) (I) LCMS analysis of relative UMP levels (per cell number) in C2C12 cells treated with CB-839 for 24h in the presence and absence of 20mM aspartate, (n=3) (J) Proliferation/survival rates of C2C12 cells cultured in 0.1mM Glutamine or with 1μM CB-839 in the presence and absence of nucleotide precursors: 200μM hypoxanthine, adenine, guanine, 100μM thymine or 400μM uridine. (n=3).

All figures denote mean ± SD unless indicated otherwise.

* $p \leq 0.05$, ** $p \leq 0.01$, *** $p \leq 0.001$.

See also (Figure S5)

Figure S5. Cytosolic aspartate is limiting for nucleotide biosynthesis under glutaminase inhibition

Figure S5 Legends: (A) Schematic overview of potential fates of cytosolic aspartate. Aspartate is a proteinogenic amino acid (red) that could aspartate undergo transaminations (green) to support non-essential amino acid biosynthesis, oxidize cytosolic NADH through malate-aspartate shuttle and recycle back to mitochondria to fuel TCA cycle. 5) Asns enzyme produces asparagine in the cytosol (blue) consuming aspartate, glutamine and ATP. 6) Aspartate is acetylated to make N-acetylaspartate (gray). 7) Aspartate is an essential component of purine and pyrimidine biosynthesis (orange). (B) GCMS analysis of endogenous intracellular N-acetylaspartate (NAA) in C2C12 and LLC1 cells (n=3). (C) mRNA expressions of genes involved in amino acid metabolism in cells cultured for 24h in the presence and absence of 4mM glutamine; fold change compared to NTC+4mMGln (n=3), medians are shown. +=4mM Gln, -=0.1mM Gln (D) Aspartate undergoes transaminations (Got1/2) to support amino acid biosynthesis, TCA cycle and NADH oxidation. TCA substrates or amino acids also undergo transaminations to produce aspartate. Experiments with using AOA or siGot1/2 may underlie which end product is most limiting. (E) Proliferation/survival rates of AGC1-KD C2C12, LLC1 and AL1376 cells treated with 0.1mM glutamine or 1µM CB-839 in the presence and absence of 20mM aspartate, 1mM or 0.1mM of a mixture of non-essential amino acids containing serine, glycine, alanine, aspartate, asparagine, proline, and glutamate or 0.3mM AOA (n=3). (F) Relative enrichment of most abundant isotopomers of TCA intermediates labelled from [U-13C]aspartate in low glutamine, normalized to individual M+4 aspartate enrichement (n=3) (G) Relative enrichment of most abundant isotopomers of TCA intermediates labelled from [U-13C]glutamate in low glutamine, normalized to individual M+5 glutamate enrichement (n=3) (H) Proliferation/survival rates of AGC1-KD C2C12, LLC1 and AL1376 cells treated with 0.1mM glutamine or with 1µM CB-839 in the presence and absence of 20mM aspartate, 2mM dimethylalpha-ketoglutarate (d-aKG), 2mM sodium pyruvate (NaPyr), 0.3mM AOA (1mM for AL1376 cells) or siRNA targeting Got1 and Got2 (n=3). (I) Aspartate is involved in both purine and pyrimidine biosynthesis pathways. Adenine, guanine and hypoxanthine nucleosides could salvage purine nucleotides while thymine and uridine could salvage pyrimidines. (J) Proliferation/survival rates of LLC1 and AL1376 cells cultured in 0.1mM Glutamine in the presence and absence of nucleotide precursors: 200µM hypoxanthine, adenine, guanine, 100µM thymine or 400µM uridine. (n=3).

All figures denote mean ± SDs unless indicated otherwise.

Figure 7. AGC1-deficiency sensitizes tumors to CB-839 treatment
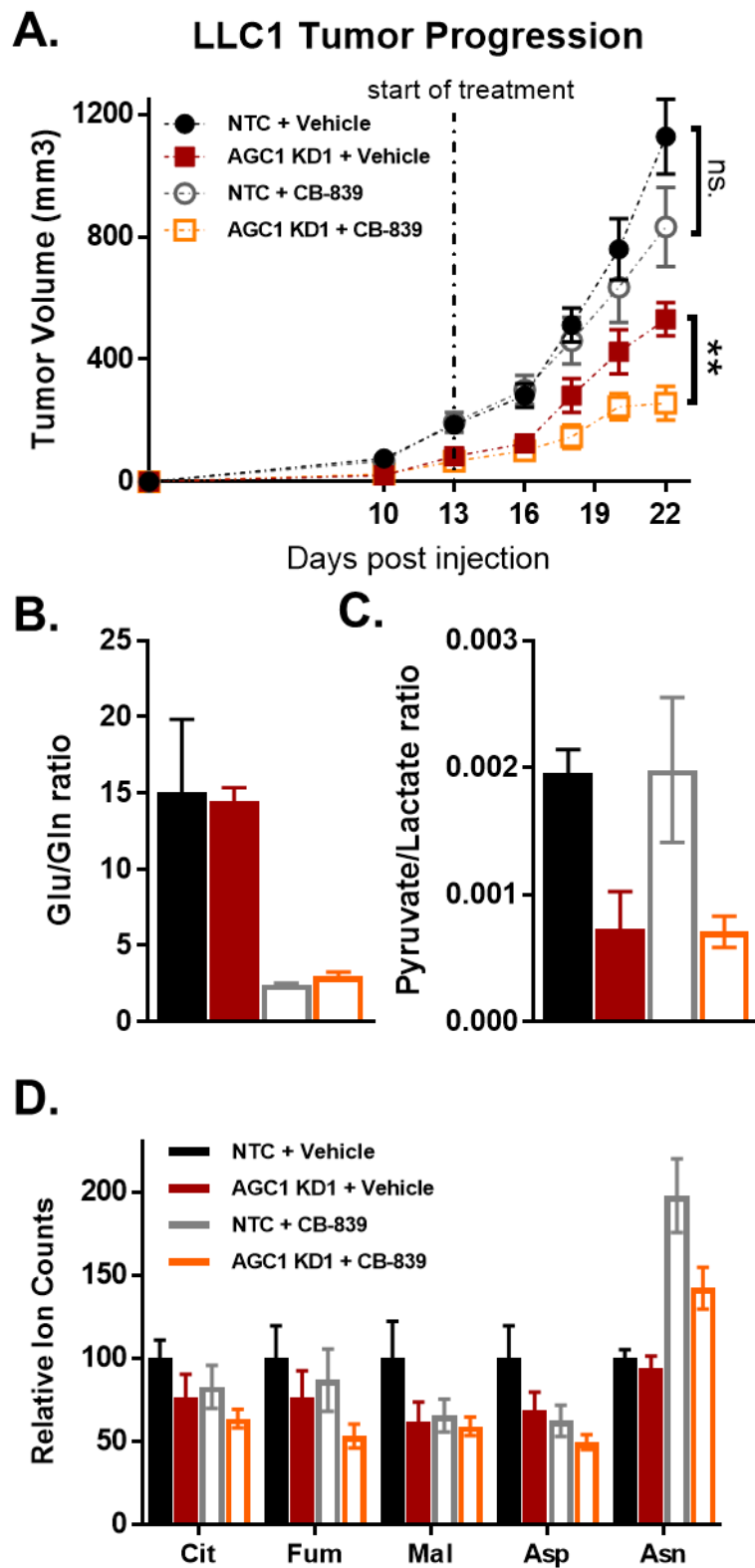
Figure 7 Legends: (A) Growth of LLC1 tumors in C56BL/6 mice flanks through the course of the experiment before and after the 200mg/kg/twice daily CB-839 treatment started (n≥6). (B) Glutamate (Glu) to Glutamine (Gln) ratio from tumors (n≥5). (C) Pyruvate to Lactate ratio from tumors (n≥5). (D) TCA intermediates and asparagine levels in tumors, normalized to valine (n≥5).
All figures denote mean ± SEM.
* p ≤ 0.05, ** p ≤ 0.01, *** p ≤ 0.001.
See also (Figure S6, S7)

Figure S6. AGC1 knock-down reduces LLC1 allograft tumor growth
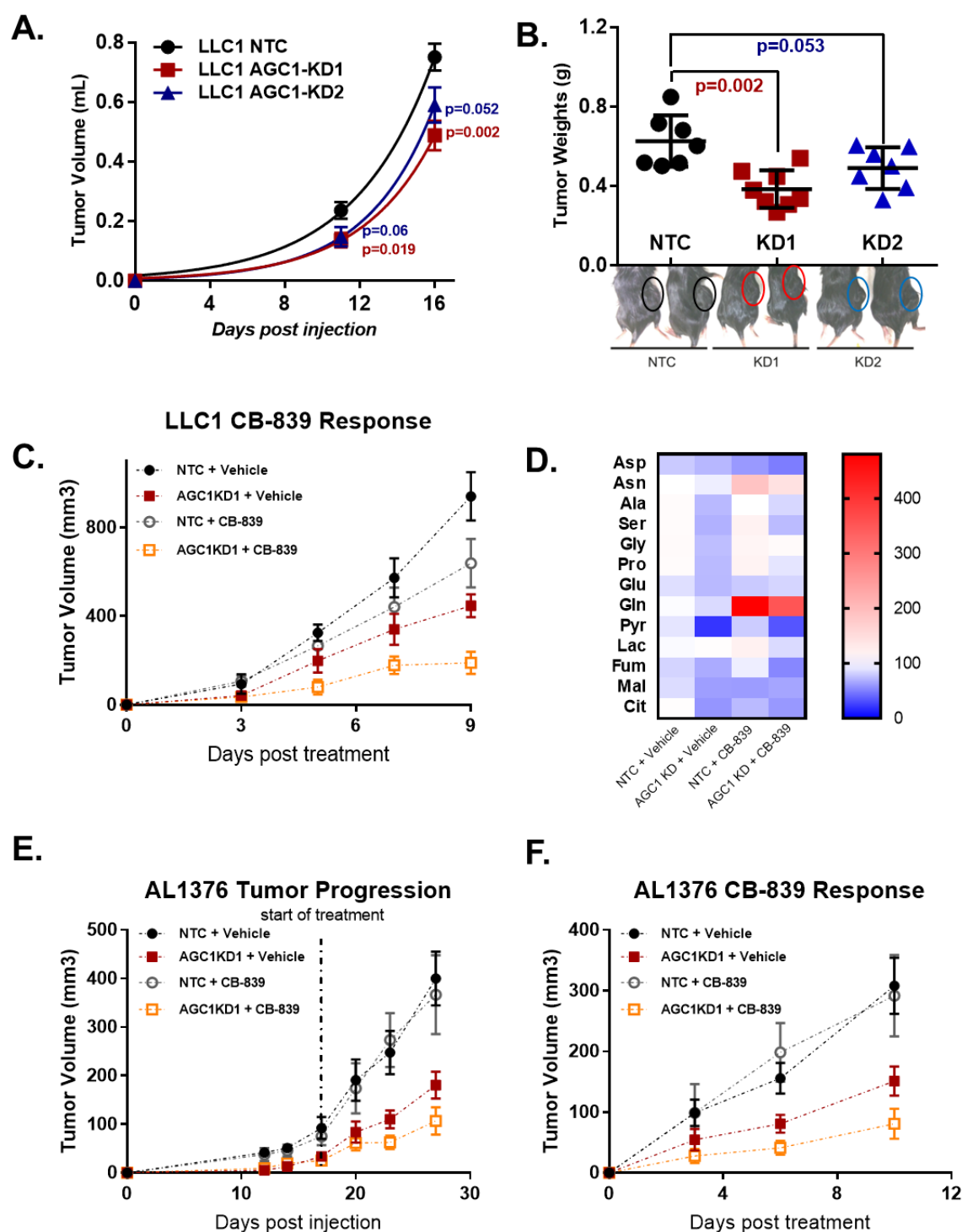
Figure S6 Legends: (A) Tumor volumes of LLC1 allografts in flanks of C56BL/6 mice. (B) Tumor weights of LLC1 allograft at day17 after injection. (C) Growth of LLC1 tumors in C56BL/6 mice flanks after the 200mg/kg/twice daily CB-839 treatment started (n≥6), mean ± SEMs are denoted. (D) Non-essential amino acids and TCA intermediates from tumors, normalized to valine; ; percent change compared to vehicle treated NTC (n≥5), medians are shown. (E) Growth of AL1376 tumors in C56BL/6 mice flanks through the course of the experiment before and after the 200mg/kg/twice daily CB-839 treatment started (n≥6). (F) Growth of AL1376 tumors in C56BL/6 mice flanks after the 200mg/kg/twice daily CB-839 treatment started (n≥6), mean ± SEMs are denoted.

Figure S7. AGC1 is expressed in several human tumors and CB-839 treatment synergizes with AGC1 knockdown in pancreas and lung cancer cell lines
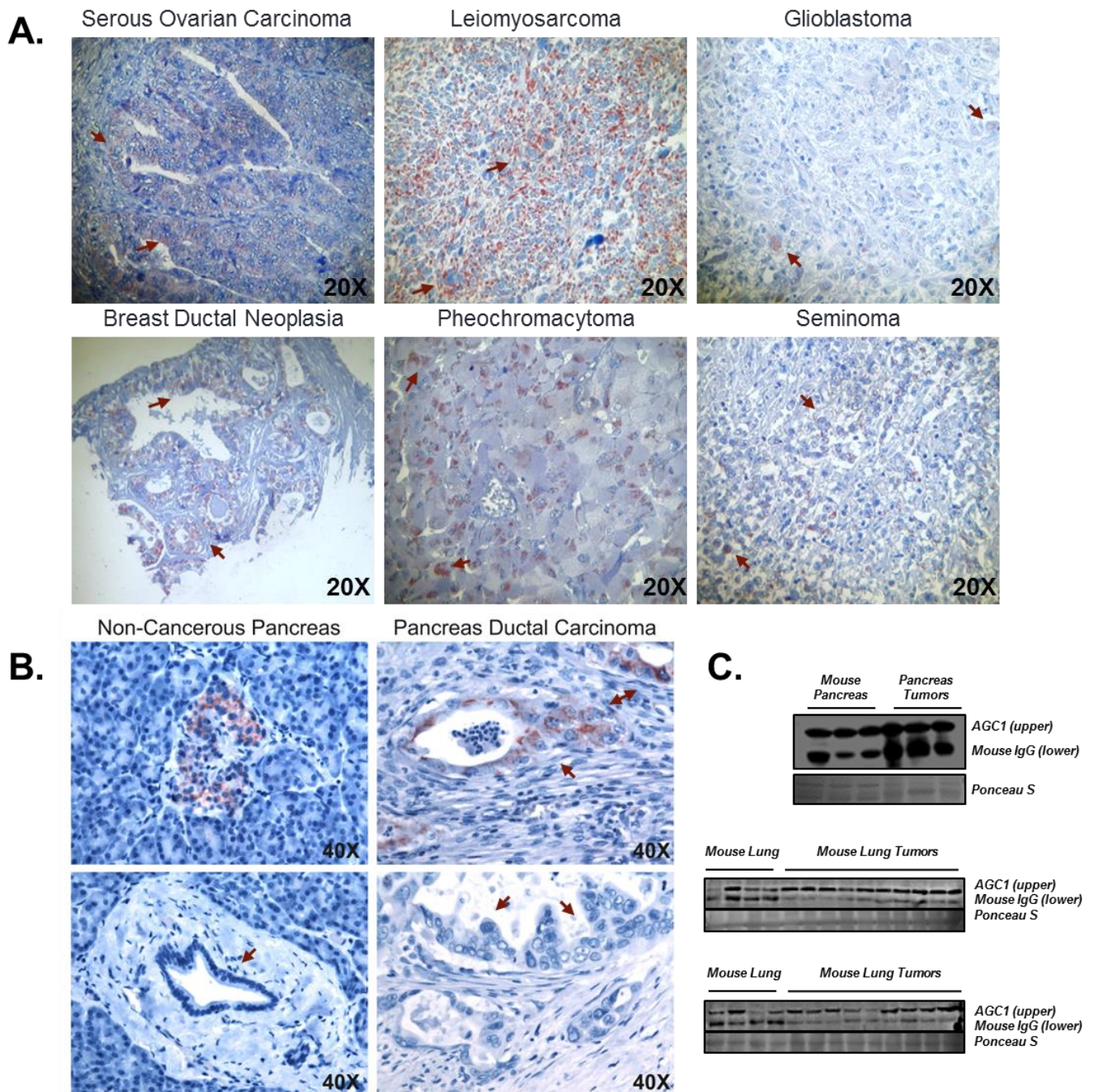
Figure S7 Legends: (A) Immunohistochemistry staining for AGC1 in human tissue microarray array (TMA). (B) Representative pictures from healthy and cancerous human pancreas sections (n=5), highlighting AGC1 expression in pancreatic beta islets [above left], normal duct [below left] or ductal carcinoma [right; above and below]. (C) AGC1 expression in pancreas (above) and lung (below) tumors from KrasG12D, p53-/- mouse models.

REFERENCES

Ahn, C.S., and Metallo, C.M. (2015). Mitochondria as biosynthetic factories for cancer proliferation. Cancer & metabolism *3*, 1.

Amoedo, N.D., Punzi, G., Obre, E., Lacombe, D., De Grassi, A., Pierri, C.L., and Rossignol, R. (2016). AGC1/2, the mitochondrial aspartate-glutamate carriers. Biochimica et biophysica acta *1863*, 2394-2412.

Begum, L., Jalil, M.A., Kobayashi, K., Iijima, M., Li, M.X., Yasuda, T., Horiuchi, M., del Arco, A., Satrustegui, J., and Saheki, T. (2002). Expression of three mitochondrial solute carriers, citrin, aralar1 and ornithine transporter, in relation to urea cycle in mice. Biochimica et biophysica acta *1574*, 283-292.

Biancur, D.E., Paulo, J.A., Malachowska, B., Del Rey, M.Q., Sousa, C.M., Wang, X., Sohn, A.S.W., Chu, G.C., Gygi, S.P., Harper, J.W., et al. (2017). Compensatory metabolic networks in pancreatic cancers upon perturbation of glutamine metabolism. Nature communications *8*, 15965.

Birsoy, K., Wang, T., Chen, W.W., Freinkman, E., Abu-Remaileh, M., and Sabatini, D.M. (2015). An Essential Role of the Mitochondrial Electron Transport Chain in Cell Proliferation Is to Enable Aspartate Synthesis. Cell *162*, 540-551.

Cassago, A., Ferreira, A.P., Ferreira, I.M., Fornezari, C., Gomes, E.R., Greene, K.S., Pereira, H.M., Garratt, R.C., Dias, S.M., and Ambrosio, A.L. (2012). Mitochondrial localization and structure-based phosphate activation mechanism of Glutaminase C with implications for cancer metabolism. Proceedings of the National Academy of Sciences of the United States of America *109*, 1092-1097.

Cheng, T., Sudderth, J., Yang, C., Mullen, A.R., Jin, E.S., Mates, J.M., and DeBerardinis, R.J. (2011). Pyruvate carboxylase is required for glutamine-independent growth of tumor cells. Proceedings of the National Academy of Sciences of the United States of America *108*, 8674-8679.

Christensen, C.E., Karlsson, M., Winther, J.R., Jensen, P.R., and Lerche, M.H. (2014). Non-invasive in-cell determination of free cytosolic [NAD+]/[NADH] ratios using hyperpolarized glucose show large variations in metabolic phenotypes. The Journal of biological chemistry *289*, 2344-2352.

Cory, J.G., and Cory, A.H. (2006). Critical roles of glutamine as nitrogen donors in purine and pyrimidine nucleotide synthesis: asparaginase treatment in childhood acute lymphoblastic leukemia. In vivo *20*, 587-589.

Davidson, S.M., Papagiannakopoulos, T., Olenchock, B.A., Heyman, J.E., Keibler, M.A., Luengo, A., Bauer, M.R., Jha, A.K., O'Brien, J.P., Pierce, K.A., et al. (2016). Environment Impacts the Metabolic Dependencies of Ras-Driven Non-Small Cell Lung Cancer. Cell metabolism *23*, 517-528.

DeBerardinis, R.J., and Chandel, N.S. (2016). Fundamentals of cancer metabolism. Science advances *2*, e1600200.

del Arco, A., Morcillo, J., Martinez-Morales, J.R., Galian, C., Martos, V., Bovolenta, P., and Satrustegui, J. (2002). Expression of the aspartate/glutamate mitochondrial carriers aralar1 and citrin during development and in adult rat tissues. European journal of biochemistry *269*, 3313-3320.

Dixon, S.J., Patel, D.N., Welsch, M., Skouta, R., Lee, E.D., Hayano, M., Thomas, A.G., Gleason, C.E., Tatonetti, N.P., Slusher, B.S., et al. (2014). Pharmacological inhibition of cystine-glutamate exchange induces endoplasmic reticulum stress and ferroptosis. eLife *3*, e02523.

Falk, M.J., Li, D., Gai, X., McCormick, E., Place, E., Lasorsa, F.M., Otieno, F.G., Hou, C., Kim, C.E., Abdel-Magid, N., et al. (2014). AGC1 Deficiency Causes Infantile Epilepsy, Abnormal Myelination, and Reduced N-Acetylaspartate. JIMD reports *14*, 77-85.

Greenhouse, W.V., and Lehninger, A.L. (1976). Occurrence of the malate-aspartate shuttle in various tumor types. Cancer research *36*, 1392-1396.

Greenhouse, W.V., and Lehninger, A.L. (1977). Magnitude of malate-aspartate reduced nicotinamide adenine dinucleotide shuttle activity in intact respiring tumor cells. Cancer research *37*, 4173-4181.

Gross, M.I., Demo, S.D., Dennison, J.B., Chen, L., Chernov-Rogan, T., Goyal, B., Janes, J.R., Laidig, G.J., Lewis, E.R., Li, J., et al. (2014). Antitumor activity of the glutaminase inhibitor CB-839 in triple-negative breast cancer. Molecular cancer therapeutics *13*, 890-901.

Gui, D.Y., Sullivan, L.B., Luengo, A., Hosios, A.M., Bush, L.N., Gitego, N., Davidson, S.M., Freinkman, E., Thomas, C.J., and Vander Heiden, M.G. (2016). Environment Dictates Dependence on Mitochondrial Complex I for NAD+ and Aspartate Production and Determines Cancer Cell Sensitivity to Metformin. Cell metabolism *24*, 716-727.

Heart, E., Cline, G.W., Collis, L.P., Pongratz, R.L., Gray, J.P., and Smith, P.J. (2009). Role for malic enzyme, pyruvate carboxylation, and mitochondrial malate import in glucose-stimulated insulin secretion. American journal of physiology. Endocrinology and metabolism *296*, E1354-1362.

Hosios, A.M., Hecht, V.C., Danai, L.V., Johnson, M.O., Rathmell, J.C., Steinhauser, M.L., Manalis, S.R., and Vander Heiden, M.G. (2016). Amino Acids Rather than Glucose Account for the Majority of Cell Mass in Proliferating Mammalian Cells. Developmental cell *36*, 540-549.

Jalil, M.A., Begum, L., Contreras, L., Pardo, B., Iijima, M., Li, M.X., Ramos, M., Marmol, P., Horiuchi, M., Shimotsu, K., et al. (2005). Reduced N-acetylaspartate levels in mice lacking aralar, a brain- and muscle-type mitochondrial aspartate-glutamate carrier. The Journal of biological chemistry *280*, 31333-31339.

Kim, J., Hu, Z., Cai, L., Li, K., Choi, E., Faubert, B., Bezwada, D., Rodriguez-Canales, J., Villalobos, P., Lin, Y.F., et al. (2017). CPS1 maintains pyrimidine pools and DNA synthesis in KRAS/LKB1-mutant lung cancer cells. Nature *546*, 168-172.

Krall, A.S., Xu, S., Graeber, T.G., Braas, D., and Christofk, H.R. (2016). Asparagine promotes cancer cell proliferation through use as an amino acid exchange factor. Nature communications *7*, 11457.

Lane, A.N., and Fan, T.W. (2015). Regulation of mammalian nucleotide metabolism and biosynthesis. Nucleic acids research *43*, 2466-2485.

Lewis, C.A., Parker, S.J., Fiske, B.P., McCloskey, D., Gui, D.Y., Green, C.R., Vokes, N.I., Feist, A.M., Vander Heiden, M.G., and Metallo, C.M. (2014). Tracing compartmentalized NADPH metabolism in the cytosol and mitochondria of mammalian cells. Molecular cell *55*, 253-263.

Lunt, S.Y., and Vander Heiden, M.G. (2011). Aerobic glycolysis: meeting the metabolic requirements of cell proliferation. Annual review of cell and developmental biology *27*, 441-464.

Mayers, J.R., Torrence, M.E., Danai, L.V., Papagiannakopoulos, T., Davidson, S.M., Bauer, M.R., Lau, A.N., Ji, B.W., Dixit, P.D., Hosios, A.M., et al. (2016). Tissue of origin dictates branched-chain amino acid metabolism in mutant Kras-driven cancers. Science *353*, 1161-1165.

Mayers, J.R., Wu, C., Clish, C.B., Kraft, P., Torrence, M.E., Fiske, B.P., Yuan, C., Bao, Y., Townsend, M.K., Tworoger, S.S., et al. (2014). Elevation of circulating branched-chain amino acids is an early event in human pancreatic adenocarcinoma development. Nature medicine *20*, 1193-1198.

McKenna, M.C., Waagepetersen, H.S., Schousboe, A., and Sonnewald, U. (2006). Neuronal and astrocytic shuttle mechanisms for cytosolic-mitochondrial transfer of reducing equivalents: current evidence and pharmacological tools. Biochemical pharmacology *71*, 399-407.

Metallo, C.M., Gameiro, P.A., Bell, E.L., Mattaini, K.R., Yang, J., Hiller, K., Jewell, C.M., Johnson, Z.R., Irvine, D.J., Guarente, L., et al. (2011). Reductive glutamine metabolism by IDH1 mediates lipogenesis under hypoxia. Nature *481*, 380-384.

Muir, A., Danai, L.V., Gui, D.Y., Waingarten, C.Y., Lewis, C.A., Vander Heiden, M.G. (2017). Environmental cystine drives glutamine anaplerosis and sensitizes cancer cells to glutaminase inhibition. eLife 2017;6:e27713

Mullen, A.R., Hu, Z., Shi, X., Jiang, L., Boroughs, L.K., Kovacs, Z., Boriack, R., Rakheja, D., Sullivan, L.B., Linehan, W.M., et al. (2014). Oxidation of alpha-ketoglutarate is required for reductive carboxylation in cancer cells with mitochondrial defects. Cell reports *7*, 1679-1690.

Okazaki, A., Gameiro, P.A., Christodoulou, D., Laviollette, L., Schneider, M., Chaves, F., Stemmer-Rachamimov, A., Yazinski, S.A., Lee, R., Stephanopoulos, G., et al. (2017). Glutaminase and poly(ADP-ribose) polymerase inhibitors suppress pyrimidine synthesis and VHL-deficient renal cancers. The Journal of clinical investigation *127*, 1631-1645.

Palmieri, F. (2013). The mitochondrial transporter family SLC25: identification, properties and physiopathology. Molecular aspects of medicine *34*, 465-484.

Palmieri, L., Pardo, B., Lasorsa, F.M., del Arco, A., Kobayashi, K., Iijima, M., Runswick, M.J., Walker, J.E., Saheki, T., Satrustegui, J., et al. (2001). Citrin and aralar1 are Ca(2+)-stimulated aspartate/glutamate transporters in mitochondria. The EMBO journal *20*, 5060-5069.

Pochini, L., Scalise, M., Galluccio, M., and Indiveri, C. (2014). Membrane transporters for the special amino acid glutamine: structure/function relationships and relevance to human health. Frontiers in chemistry *2*, 61.

Profilo, E., Pena-Altamira, L.E., Corricelli, M., Castegna, A., Danese, A., Agrimi, G., Petralla, S., Giannuzzi, G., Porcelli, V., Sbano, L., et al. (2017). Down-regulation of the mitochondrial aspartate-glutamate carrier isoform 1 AGC1 inhibits proliferation and N-acetylaspartate synthesis in Neuro2A cells. Biochimica et biophysica acta *1863*, 1422-1435.

Ratnikov, B., Aza-Blanc, P., Ronai, Z.A., Smith, J.W., Osterman, A.L., and Scott, D.A. (2015). Glutamate and asparagine cataplerosis underlie glutamine addiction in melanoma. Oncotarget *6*, 7379-7389.

Rivera, S., Lopez-Soriano, F.J., Azcon-Bieto, J., and Argiles, J.M. (1987). Blood amino acid compartmentation in mice bearing Lewis lung carcinoma. Cancer research *47*, 5644-5646.

Rubi, B., del Arco, A., Bartley, C., Satrustegui, J., and Maechler, P. (2004). The malate-aspartate NADH shuttle member Aralar1 determines glucose metabolic fate, mitochondrial activity, and insulin secretion in beta cells. The Journal of biological chemistry *279*, 55659-55666.

Saheki, T., Kobayashi, K., Iijima, M., Nishi, I., Yasuda, T., Yamaguchi, N., Gao, H.Z., Jalil, M.A., Begum, L., and Li, M.X. (2002). Pathogenesis and pathophysiology of citrin (a mitochondrial aspartate glutamate carrier) deficiency. Metabolic brain disease *17*, 335-346.

Sakurai, T., Ramoz, N., Barreto, M., Gazdoiu, M., Takahashi, N., Gertner, M., Dorr, N., Gama Sosa, M.A., De Gasperi, R., Perez, G., et al. (2010). Slc25a12 disruption alters myelination and neurofilaments: a model for a hypomyelination syndrome and childhood neurodevelopmental disorders. Biological psychiatry *67*, 887-894.

Sanjana, N.E., Shalem, O., Zhang, F. (2014) Improved lentiviral vectors and genome-wide libraries for CRISPR screening. Nature Methods

Shalem, O., Sanjana, N.E., Hartenian, E., Shi, X., Scott, D.A., Mikkelsen, T., Heckl, D., Ebert, B.L., Root, D.E., Doench, J.G., Zhang, F. (2014). Science, 343, 83-7

Sullivan, L.B., Gui, D.Y., Hosios, A.M., Bush, L.N., Freinkman, E., and Vander Heiden, M.G. (2015). Supporting Aspartate Biosynthesis Is an Essential Function of Respiration in Proliferating Cells. Cell *162*, 552-563.

Thangaratnarajah, C., Ruprecht, J.J., and Kunji, E.R. (2014). Calcium-induced conformational changes of the regulatory domain of human mitochondrial aspartate/glutamate carriers. Nature communications *5*, 5491.

Vander Heiden, M.G., Cantley, L.C., and Thompson, C.B. (2009). Understanding the Warburg effect: the metabolic requirements of cell proliferation. Science *324*, 1029-1033.

Vander Heiden, M.G., and DeBerardinis, R.J. (2017). Understanding the Intersections between Metabolism and Cancer Biology. Cell *168*, 657-669.

Vyas, S., Zaganjor, E., Haigis, M.C. (2016). Mitochondria and Cancer. Cell 166, 555-676

Warburg, O. (1956). On the origin of cancer cells. Science *123*, 309-314.

Wie-Xing, Z., Rabinowitz, J.D., and White, E. (2016). Mitochondria and Cancer. Molecular cell 61, 667-676

Wibom, R., Lasorsa, F.M., Tohonen, V., Barbaro, M., Sterky, F.H., Kucinski, T., Naess, K., Jonsson, M., Pierri, C.L., Palmieri, F., et al. (2009). AGC1 deficiency associated with global cerebral hypomyelination. The New England journal of medicine *361*, 489-495.

Williamson, D.H., Lund, P., and Krebs, H.A. (1967). The redox state of free nicotinamide-adenine dinucleotide in the cytoplasm and mitochondria of rat liver. The Biochemical journal *103*, 514-527.

Wise, D.R., and Thompson, C.B. (2010). Glutamine addiction: a new therapeutic target in cancer. Trends in biochemical sciences *35*, 427-433.

Yasuda, T., Yamaguchi, N., Kobayashi, K., Nishi, I., Horinouchi, H., Jalil, M.A., Li, M.X., Ushikai, M., Iijima, M., Kondo, I., et al. (2000). Identification of two novel mutations in the SLC25A13 gene and detection of seven mutations in 102 patients with adult-onset type II citrullinemia. Human genetics *107*, 537-545.

Yuneva, M., Zamboni, N., Oefner, P., Sachidanandam, R., and Lazebnik, Y. (2007). Deficiency in glutamine but not glucose induces MYC-dependent apoptosis in human cells. The Journal of cell biology *178*, 93-105.

Yuneva, M.O., Fan, T.W., Allen, T.D., Higashi, R.M., Ferraris, D.V., Tsukamoto, T., Mates, J.M., Alonso, F.J., Wang, C., Seo, Y., et al. (2012). The metabolic profile of tumors depends on both the responsible genetic lesion and tissue type. Cell metabolism *15*, 157-170.

Zhang, J., Fan, J., Venneti, S., Cross, J.R., Takagi, T., Bhinder, B., Djaballah, H., Kanai, M., Cheng, E.H., Judkins, A.R., et al. (2014). Asparagine plays a critical role in regulating cellular adaptation to glutamine depletion. Molecular cell *56*, 205-218.